JBC ARTICLE

TRIM24 protein promotes and TRIM32 protein inhibits cardiomyocyte hypertrophy via regulation of dysbindin protein levels

Received for publication, August 9, 2016, and in revised form, April 28, 2017 Published, Papers in Press, May 2, 2017, DOI 10.1074/jbc.M116.752543

Ankush Borlepawar[‡§1], **Ashraf Yusuf Rangrez**[‡§1,2,3], **Alexander Bernt**[‡§], **Lynn Christen**[‡], **Samuel Sossalla**[‡§], **Derk Frank**[‡§2], **and Norbert Frey**[‡§2,4]

From the [‡]*Department of Internal Medicine III (Cardiology, Angiology, Intensive Care), University Medical Center Kiel and the* [§]*DZHK (German Centre for Cardiovascular Research), Partner Site Hamburg/Kiel/Lübeck, 24105 Kiel, Germany*

Edited by George N. DeMartino

We have previously shown that dysbindin is a potent inducer of cardiomyocyte hypertrophy via activation of Rho-dependent serum-response factor (SRF) signaling. We have now performed a yeast two-hybrid screen using dysbindin as bait against a cardiac cDNA library to identify the cardiac dysbindin interactome. Among several putative binding proteins, we identified tripartite motif-containing protein 24 (TRIM24) and confirmed this interaction by co-immunoprecipitation and co-immunostaining. Another tripartite motif (TRIM) family protein, TRIM32, has been reported earlier as an E3 ubiquitin ligase for dysbindin in skeletal muscle. Consistently, we found that TRIM32 also degraded dysbindin in neonatal rat ventricular cardiomyocytes as well. Surprisingly, however, TRIM24 did not promote dysbindin decay but rather protected dysbindin against degradation by TRIM32. Correspondingly, TRIM32 attenuated the activation of SRF signaling and hypertrophy due to dysbindin, whereas TRIM24 promoted these effects in neonatal rat ventricular cardiomyocytes. This study also implies that TRIM32 is a key regulator of cell viability and apoptosis in cardiomyocytes via simultaneous activation of p53 and caspase-3/-7 and inhibition of X-linked inhibitor of apoptosis. In conclusion, we provide here a novel mechanism of post-translational regulation of dysbindin and hypertrophy via TRIM24 and TRIM32 and show the importance of TRIM32 in cardiomyocyte apoptosis *in vitro*.

Cardiomyocyte hypertrophy is a complex process with involvement of various signaling pathways like calcineurin-nuclear factor of activated T-cells, PI3K/Akt/GSK-3, G protein-coupled receptors, MAPK, and RhoA-SRF[5]-mediated pathways (1–4). Myozap, an intercalated disc protein, was recently found to activate RhoA-SRF signaling and hypertrophy in cardiomyocytes (5–7). In the quest of decoding more players in this hypertrophic signaling axis, we identified dysbindin as a direct binding partner of Myozap (8). Dysbindin has so far mostly been studied in neuroscience, focusing largely on its role in schizophrenia susceptibility and neuronal outgrowth (9–13). From a cardiac perspective, however, dysbindin has recently been shown to be a potent inducer of SRF signaling via a direct interaction with the small GTPase RhoA (8). This led us to seek new cardiac binding partners of dysbindin, to potentially disclose other proteins involved in SRF signaling in cardiomyocytes, and to study their effects on dysbindin and cardiac hypertrophy.

The tripartite motif (TRIM) is a conserved RBCC (RING-B-box coiled-coil) domain-containing protein family (14, 15), which expanded rapidly during vertebrate evolution, now including more than 60 known members in metazoans (16). The TRIM protein superfamily is known to consist of major E3 ubiquitin ligases, playing an important role in post-translational modifications of multiple proteins (17). Yet, little is known about the cardiac functions of this vital protein family despite their significant expression levels in the heart. A few exceptions include TRIM63, TRIM55, and TRIM54, also known as "muscle ring finger (MuRF)" proteins (MuRF1, -2, and -3, respectively), that are specifically expressed in cardiac and skeletal muscle. These proteins modulate cardiac growth and function through ubiquitin-proteasome-dependent degradation of sarcomere proteins like myosin, troponin I, as well as hypertrophic signaling factors such as PKC, SRF, and IGF-1 (18–24). Moreover, mutations in the genes encoding MuRF1 and MuRF2 have been reported to cause hypertrophic cardiomyopathy by impairing protein degradation in cardiomyocytes (25–27). Genetic mutations in TRIM32, cause limb girdle

This work was supported in part by German Research Foundation (DFG) Grant RA2717/2-1 (to A. Y. R. and N. F.) and Federal Ministry of Education and Research (BMBF) e:Med Grant SYMBOL-HF (to D. F.). The authors declare that they have no conflicts of interest with the contents of this article.
This article contains supplemental Figs. S1–S6.

[1] Both authors contributed equally to this work.
[2] Supported by the DZHK (German Centre for Cardiovascular Research).
[3] To whom correspondence may be addressed: Dept. of Internal Medicine III, University Medical Center Kiel, 24105 Kiel, Germany. Tel.: 49-500-22935; Fax: 49-500-22938; E-mail: ashraf.rangrez@uk-sh.de.
[4] Supported by Deutsche Forschungsgemeinschaft Grant FR1289/5-1. To whom correspondence may be addressed: Dept. of Internal Medicine III, University Medical Center Kiel, 24105 Kiel, Germany. Tel.: 49-500-22800; Fax: 49-500-22804; E-mail: norbert.frey@uk-sh.de.

[5] The abbreviations used are: SRF, serum-response factor; XIAP, X-linked inhibitor of apoptosis; NRVCM, neonatal rat ventricular cardiomyocyte; qRT, quantitative RT; MTT, 3-(4,5-dimethylthiazol-2-yl)-2,5-diphenyltetrazolium bromide; NF, non-failing; PE, phenylephrine; DCM, dilated cardiomyopathy; HCM, hypertrophic cardiomyopathy; Y2H, yeast two-hybrid; MCC, Mander's co-localization coefficient; UPS, ubiquitin-proteasome system; PI, propidium iodide; TRIM, tripartite motif; RBCC, RING-B-box coiled-coil; co-IP, co-immunoprecipitation; TAC, transverse aortic constriction; MuRF, muscle ring finger; SRF-RE, SRF-response element; ifu, infection-forming unit.

Table 1
List of putative dysbindin-binding partners, arranged alphabetically, identified through a yeast two-hybrid screen performed using human dysbindin as bait against human cardiac cDNA library

Prey	Description	Link to genes
ALDOA	Aldolase A, fructose-bisphosphate	226
ANKRD2	Ankyrin repeat domain 2	26287
APPL1	Adaptor protein, phosphotyrosine interaction, PH domain, and leucine zipper containing 1	26060
ATP5B	ATP synthase, H^+-transporting, mitochondrial F1 complex, β-polypeptide	506
CTDNEP1	CTDNEP1 CTD nuclear envelope phosphatase 1	23399
CYB5R3	Cytochrome b_5 reductase 3	1727
EIF2B4	Eukaryotic translation initiation factor 2B, subunit 4δa, 67 kDa	8890
HADHB	Hydroxyacyl-coenzyme A dehydrogenase/3-ketoacyl-coenzyme A thiolase/enoyl-coenzyme A hydratase (trifunctional protein), β subunit	3032
LIMA1	LIM domain and actin binding 1	51474
MYH6	Myosin, heavy chain 6, cardiac muscle, α	4624
MYH7	Myosin, heavy chain 7, cardiac muscle, β	4625
NDUFB8	NADH dehydrogenase (ubiquinone) 1β subcomplex subunit 8, mitochondrial precursor	4714
NLRP1	NLR family, pyrin domain containing 1	22861
NMNAT1	Nicotinamide mononucleotide adenylyltransferase1 (EC 2.7.7.1) (NMN adenylyltransferase 1)	64802
NPPA	Natriuretic peptide precursor A	4878
OPTN	Optineurin	10133
PES1	Pescadillo homolog 1, containing BRCT domain	23481
RARG	Retinoic acid receptor, γ	5916
RHOA	*ras* homolog gene family, member A	387
SHMT1	Serine hydroxymethyltransferase 1 (soluble)	6470
SNRPN	Small nuclear ribonucleoprotein polypeptide N	6638
SNURF	SNURF SNRPN upstream reading frame	8926
TNNT2	Troponin T type 2 (cardiac)	7139
TRIM24	Transcription intermediary factor 1-α (TIF1-α) (tripartite motif-containing protein 24) (RING finger protein 82)	8805

muscular dystrophy (28) and Bardet-Biedl syndrome (29). Interestingly, Locke *et al.* (30) reported that TRIM32 degrades dysbindin via the ubiquitin proteasome system (UPS) in cultured myoblasts. Recently, Chen *et al.* (31) have shown that TRIM32 prevents pathological cardiac hypertrophy *in vivo* in mice. However, it is unclear whether TRIM32 affects cardiac dysbindin levels and/or molecular signaling in cardiomyocyte hypertrophy.

In this study, we focused on TRIM24, a newly identified TRIM family member as a binding partner of dysbindin in our yeast two-hybrid (Y2H) screen. TRIM24 has been studied thus far only in the context of cancer (32–34). TRIM24 is known to be interacting with tumor protein 53 (p53), leading to its degradation by ubiquitination and hence affecting genomic stability, cell cycle arrest, and apoptosis (35). It is also known for its function as a transcriptional intermediary factor or transcriptional activator for various genes (36, 37), its interaction with several nuclear receptors (38), an interaction with histone H3 (39), as well as a marker in carcinoma and glioma progression (40, 41). However, to the best of our knowledge, the cardiac function of TRIM24 has not yet been determined. This study is thus centered on the cardiac dysbindin-TRIM24-TRIM32 interaction, to elucidate the control of dysbindin levels and function by TRIM24/32 in cardiomyocytes.

Results

TRIM24 and TRIM32 interact with dysbindin in cardiomyocytes

We have recently demonstrated that dysbindin is a potent inducer of RhoA-SRF-mediated cardiac hypertrophy (8). In search of new cardiac-specific binding partners of dysbindin, yeast two-hybrid (Y2H) screening was performed, with dysbindin as bait and human cardiac cDNA library as prey. This screening revealed TRIM24, a tripartite motif-containing family E3 ubiquitin ligase, as one of the potential interaction partners of dysbindin along with several others (Table 1). TRIM32, another TRIM E3 ligase, has earlier been reported to interact with dysbindin in skeletal muscle cells through its coiled-coil domain (30). Thus, we first determined the potential interaction of these two TRIM family member proteins with dysbindin by co-immunoprecipitation (co-IP) in HEK293A cells. We successfully pulled down dysbindin with TRIM24/32 and vice versa (Fig. 1, *A*–*D*). We also validated this interaction in neonatal rat ventricular cardiomyocytes (NRVCMs), where we could only pull down TRIM24/32 using an antibody against dysbindin (Fig. 1, *E* and *F*). Moreover, to check the domain specificity of TRIM24-dysbindin interaction, we performed Co-IP experiments in HEK293A cells by co-transfecting TRIM24 with several dysbindin fragments as depicted in supplemental Fig. S1*A*. It was seen that the coiled-coil domain of dysbindin is the minimum required domain for dysbindin-TRIM24 interaction (supplemental Fig. S1*B*).

Interestingly, the tissue distribution pattern of TRIM24 and TRIM32 in mice showed significant expression at the mRNA level in the heart in addition to various other tissues, which further implies a cardiac role (supplemental Fig. S1*C*). However, at the protein level, TRIM24 was maximally expressed in skeletal muscle, whereas TRIM32 was prominently expressed in the brain (supplemental Fig. S1*D*). Subcellular localization of both TRIMs and their co-localization with dysbindin were then determined by high resolution confocal imaging in NRVCMs by co-immunostaining dysbindin with either TRIM24- or TRIM32-specific antibodies. Similar to dysbindin, endogenous TRIM24 was found to be prominently located in the nuclei and perinuclear region (Fig. 1*G*, *upper panel*), and, when co-expressed with dysbindin, it was also seen scattered in the cytoplasm (supplemental Fig. S1*E*, *upper panel*). On the one hand, endogenous TRIM32 was localized throughout the cell but was concentrated in the perinuclear region (Fig. 1*G*, *lower panel*). We measured robust Mander's coefficients (representing above 90% co-localization) when either endogenous or overexpressed

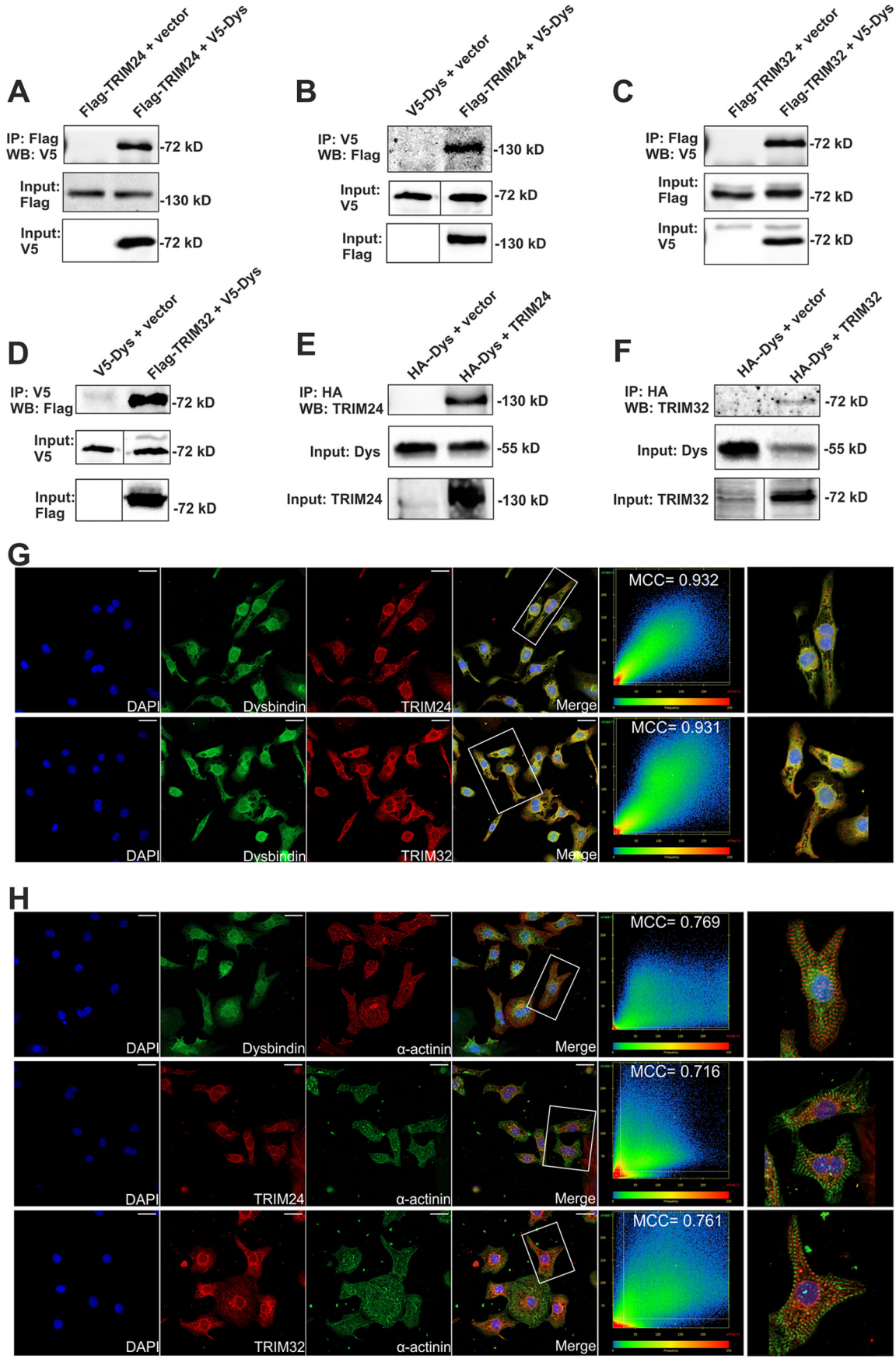
A
Flag-TRIM24 + vector
Flag-TRIM24 + V5-Dys
IP: Flag
WB: V5
-72 kD
Input:
Flag
-130 kD
Input:
V5
-72 kD
B
V5-Dys + vector
Flag-TRIM24 + V5-Dys
IP: V5
WB: Flag
-130 kD
Input:
V5
-72 kD
Input:
Flag
-130 kD
C
Flag-TRIM32 + vector
Flag-TRIM32 + V5-Dys
IP: Flag
WB: V5
-72 kD
Input:
Flag
-72 kD
Input:
V5
-72 kD
D
V5-Dys + vector
Flag-TRIM32 + V5-Dys
IP: V5
WB: Flag
-72 kD
Input:
V5
-72 kD
Input:
Flag
-72 kD
E
HA--Dys + vector
HA-Dys + TRIM24
IP: HA
WB: TRIM24
-130 kD
Input: Dys
-55 kD
Input: TRIM24
-130 kD
F
HA--Dys + vector
HA-Dys + TRIM32
IP: HA
WB: TRIM32
-72 kD
Input: Dys
-55 kD
Input: TRIM32
-72 kD
G
DAPI
Dysbindin
TRIM24
Merge
MCC= 0.932
DAPI
Dysbindin
TRIM32
Merge
MCC= 0.931
H
DAPI
Dysbindin
α-actinin
Merge
MCC= 0.769
DAPI
TRIM24
α-actinin
Merge
MCC= 0.716
DAPI
TRIM32
α-actinin
Merge
MCC= 0.761

TRIM proteins co-localize with dysbindin (93% co-localization, Fig. 1*G* and supplemental Fig. S1*C*). Knockdown of either dysbindin or TRIM24/32, on the other hand, did not result in any visible effect on subcellular localization of the respective other protein (supplemental Fig. S1, *F–I*). Furthermore, co-immunostaining of dysbindin, TRIM24, or TRIM32 with α-actinin indicated that, unlike their strong biochemical interaction with each other, these proteins only partially co-localize with sarcomeric α-actinin (Fig. 1*H*).

TRIM24 and TRIM32 are differentially regulated in cardiac hypertrophy and cardiomyopathy in vivo

Because of the known involvement of MuRF1/2, two other important TRIM family proteins, in cardiac hypertrophy and cardiomyopathy, we checked for the expression of TRIM24/32 in mouse models of cardiac hypertrophy induced either by biomechanical stress due to transverse aortic constriction (TAC) or by controlled infusion of an α-adrenergic agonist, phenylephrine (PE). Sham-operated and mice infused only with physiological saline served as the respective control groups. At protein level, TRIM24 was significantly up-regulated in PE-treated mice (Fig. 2, *A* and *B*), but its expression remained unchanged in TAC-operated mice (Fig. 2, *D* and *E*). However, TRIM24 transcript levels were unaffected in either of the mouse models (Fig. 2, *C* and *F*). TRIM32 also displayed no change in mRNA levels (Fig. 2, *C* and *F*), but its expression at the protein level was significantly reduced in both hypertrophic models (Fig. 2, *A*, *B, D,* and *E*), consistent with a post-transcriptional control on its expression. Interestingly, however, neither of the TRIM proteins was dysregulated in genetic mouse models of hypertrophy (calcineurin-transgenic mouse, supplemental Figs. S2*A* and S3*C*) nor dilated cardiomyopathy (MLP knock-out mouse, supplemental Fig. S2, *D–F*).

Furthermore, we asked whether protein expression of TRIM24 and TRIM32 is altered in human patients suffering from hypertrophic or dilated cardiomyopathy (HCM/DCM). Similar to the effects observed in hypertrophic mice, TRIM24 displayed a striking increase in both HCM and DCM heart tissues, whereas TRIM32 again showed a significant reduction in protein levels compared with non-failing (NF) human heart samples (Fig. 2, *G–L*). Thus, the consistent dysregulation of the TRIM24/32 expression in hypertrophic datasets obtained from animal models and human patients indicated possible relevance of both TRIMs in the pathogenesis of cardiac hypertrophy and cardiomyopathy, and this prompted us to further investigate their role in cardiomyocytes.

TRIM24 and TRIM32 antagonistically regulate dysbindin levels and SRF activity in NRVCMs

TRIM24 and TRIM32 are members of the TRIM protein superfamily, mostly consisting of E3 ubiquitin ligases, which contain Ring finger domains for ubiquitination of cellular proteins (16). To determine their role in dysbindin degradation, we infected several combinations of dysbindin, TRIM24, and TRIM32 adenoviruses (supplemental Fig. S3, *A*, *B, E, F, I,* and *J*) in NRVCMs in the absence or presence of either ubiquitin or MG132 (a proteasome inhibitor) or both. Interestingly, immunoblot analysis demonstrated no effect on dysbindin in the presence of TRIM24 but robust degradation in the presence of TRIM32 (Fig. 3, *A–D*), suggesting that TRIM32, but not TRIM24, acts as an E3 ubiquitin ligase of dysbindin in cardiomyocytes. Adenovirus-mediated knockdown of either TRIM24 or TRIM32 using synthetic microRNA (supplemental Fig. S3, *G, H, K,* and *L*), however, did not alter dysbindin expression (Fig. 3, *E* and *F*). Along these lines, we first confirmed that dysbindin is polyubiquitinated by ubiquitin overexpression (Fig. 3, *G* and *H*). We then analyzed the effect of proteasome inhibitor MG132 on the E3 ubiquitin ligase and ubiquitination activity of TRIM24/32. We found that the presence of TRIM24 significantly reduced ubiquitin-mediated dysbindin degradation, whereas MG132 treatment abrogated the degradation of dysbindin by ubiquitin, indicating that the dysbindin degradation is UPS-dependent (Fig. 3, *I–K*). Similarly, MG132 treatment blunted the dysbindin degradation due to TRIM32 in the presence or absence of ubiquitin (Fig. 3, *L–N*). Notably, overexpression of TRIM32 robustly increased ubiquitination of the proteins, whereas TRIM24 exhibited opposite effects (Fig. 3, *K* and *N*). Altogether, these data strongly show that TRIM32 acts as a UPS-dependent E3 ubiquitin ligase for dysbindin, whereas TRIM24 exhibits protective effects.

We have previously identified dysbindin as a robust inducer of Rho-dependent SRF signaling (8). To explore the potential effects of both TRIMs on this pathway, we overexpressed TRIM24 and TRIM32 in the absence or presence of dysbindin in NRVCMs and assessed the activation of SRF signaling using the SRF-response element (SRF-RE)-driven firefly luciferase activity. Interestingly, TRIM24 exhibited a positive effect on SRF signaling as observed with dysbindin. TRIM24 when co-expressed with dysbindin displayed an additive effect on the robust activation of SRF signaling by dysbindin (Fig. 4*A*). To the contrary, overexpressed TRIM32 did not show significant effect on SRF signaling compared with control; notwithstanding, it strongly diminished the induction of SRF signaling by

Figure 1. TRIM24 and TRIM32 interact with cardiac dysbindin. HEK293A cells were co-transfected with V5-tagged dysbindin and FLAG-tagged TRIM24 or TRIM32. Empty vectors transfected with either dysbindin, TRIM24, or TRIM32 were used as respective controls. Immunoprecipitation was performed using anti-V5 or FLAG tag cross-linked magnetic beads. Precipitated proteins were immunoblotted with respective antibodies. Dysbindin was found to be co-precipitated with TRIM24 (*A*) and vice versa (*B*). Similarly, TRIM32 and dysbindin pulled down each other (*C* and *D*, respectively), although no interaction was seen in control IP (*lane 1* in each blot), confirming interaction between dysbindin and TRIM24/TRIM32. We also performed co-IP by overexpressing HA-tagged dysbindin in NRVCMs and precipitated using anti-HA tag cross-linked magnetic beads. Precipitated proteins were immunoblotted with TRIM24 (*E*) and TRIM32 (*F*) antiserum. and the interaction between dysbindin and TRIM24 or TRIM32 was further validated. *Vertical black lines* in the blots indicate that the intervening lanes have been spliced out. *G,* confocal micrographs representing the co-immunostaining of endogenous dysbindin with either TRIM24 (*upper lane*) or TRIM32 (*lower lane*). *H,* co-immunostaining of native dysbindin, TRIM24, or TRIM32 with α-actinin. Nuclei were stained with DAPI, and images were captured with a Zeiss LSM800 laser-scanning microscope. Scatter plots show the analysis of co-localization as described under "Experimental procedures." *White rectangles* represent cropped areas for detailed re-acquisition. *MCC* = Mander's co-localization coefficient. *Scale bar* (shown with a *white line*), 20 μm. *IP,* immunoprecipitation; *WB,* Western blotting; *Dys,* dysbindin.

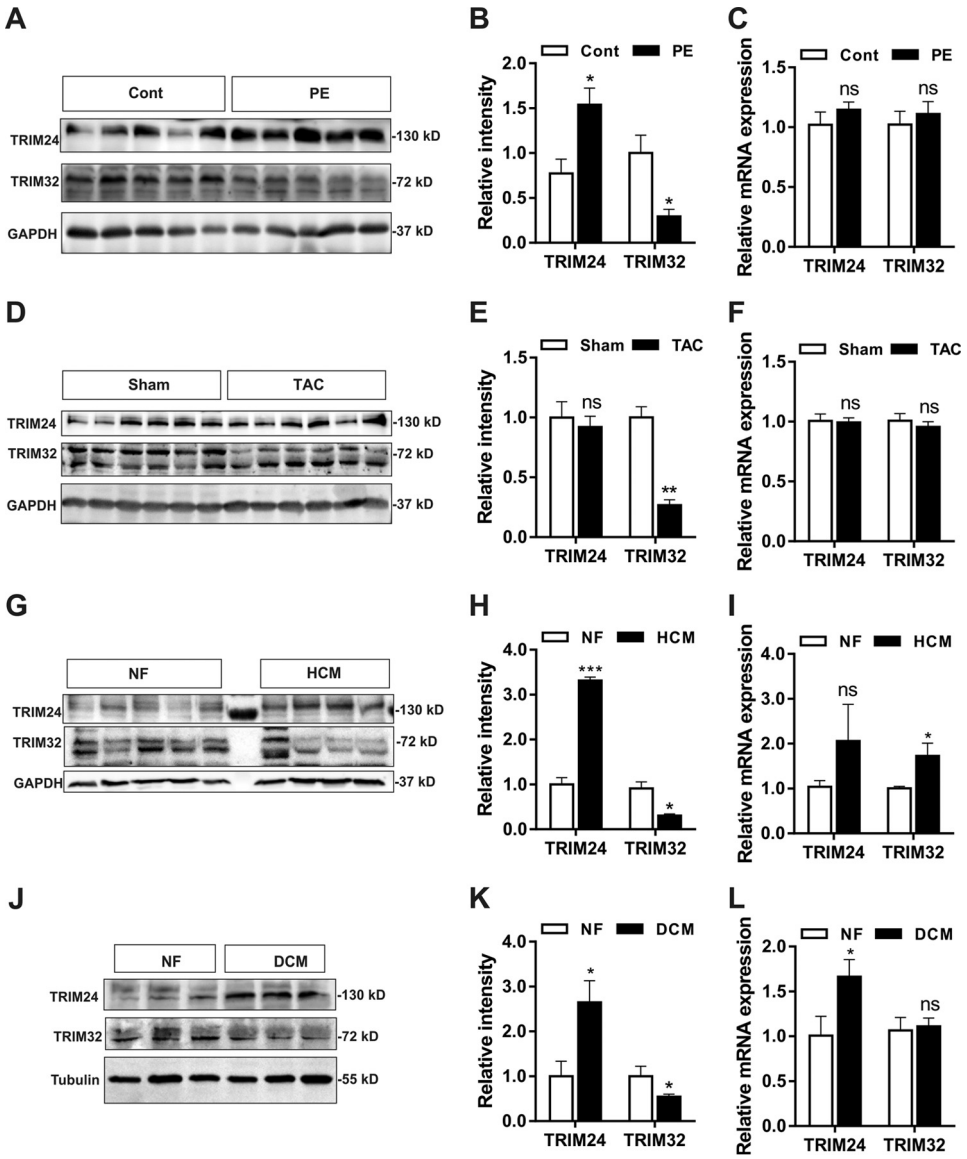

Figure 2. TRIM24 and TRIM32 are differentially regulated in cardiac hypertrophy and cardiomyopathy *in vivo*. *A,* protein expression of TRIM24 and TRIM32 in control (*PBS*) and phenylephrine (*PE*)-treated mice. Osmotic mini-pumps filled with PE (25 μg/kg body weight/min) prepared in PBS with 1 mg/ml L-ascorbate (Sigma) were implanted subcutaneously in 8-week-old C57BL/6 mice and housed for 2 weeks. Control mice group received vehicle L-ascorbate in PBS. Post 2-week implantation, protein isolated from the hearts of these mice was immunoblotted against respective TRIM antiserum. $n = 5$. Respective densitometry analysis is shown in *B*, with GAPDH as endogenous control. *C,* quantitative real-time PCR was performed to identify the transcript levels of TRIM24 and TRIM32 in PE-treated mice compared with the control mice group. *D,* protein expression of TRIM24 and TRIM32 in TAC or sham-operated mice. 8-Week-old C57BL/6 mice were subjected to TAC operations, and heart samples were used for protein isolation 2 weeks post-operation. Protein samples were immunoblotted against respective TRIM antiserum. $n = 6$. Respective densitometry analysis is shown in *E*, with GAPDH as endogenous control. *F,* transcript levels of TRIM24 and TRIM32 were determined by qRT-PCR in sham *versus* TAC-operated mouse hearts. *G,* protein expression of TRIM24 and TRIM32 in non-failing (*NF*, $n = 7$) and hypertrophic cardiomyopathy (HCM, $n = 4$)-affected human hearts. *H,* densitometric analysis was performed for respective immunoblots from *G*, with GAPDH as an endogenous loading control. *I,* quantitative real-time PCR was performed to identify the transcript levels of TRIM24 and TRIM32 in NF *versus* HCM patients. *J,* protein expression of TRIM24 and TRIM32 in non-failing (*NF*, $n = 7$) and dilated cardiomyopathy (DCM, $n = 10$) affected human hearts. *K,* densitometric analysis was performed for respective immunoblots from *J*, with tubulin as an endogenous loading control. *L,* quantitative real-time PCR was performed to identify the transcript levels of TRIM24 and TRIM32 in NF *versus* DCM patients. Statistical significance was determined using two-tailed Student's *t* test. *Error bars* show means ± S.E. *, $p < 0.05$; **, $p < 0.01$; ***, $p < 0.001$; *ns,* non-significant. *Cont,* control; *PE,* phenylephrine; *TAC,* transverse aortic constriction.

dysbindin (Fig. 4*B*). Correspondingly, knockdown of TRIM24 using a TRIM24-specific synthetic microRNA resulted in reduced SRF activation, but no significant difference was observed when this knockdown was followed by dysbindin overexpression, compared with the overexpression of dysbindin alone (Fig. 4*C*). Although knockdown of endogenous TRIM32 resulted in a significant increase of SRF-luciferase activity in the presence of dysbindin, no significant effect of TRIM32 knockdown was observed in the absence of dysbindin (Fig. 4*D*).

TRIM32 adversely affects cell viability and hypertrophy

To investigate the (patho-) physiological role of TRIM24/32, we performed comparative analyses of the effects of dysbindin, TRIM24, and TRIM32 on the growth and survival of cardiomyocytes. The pro-hypertrophic effect of dysbindin expres-

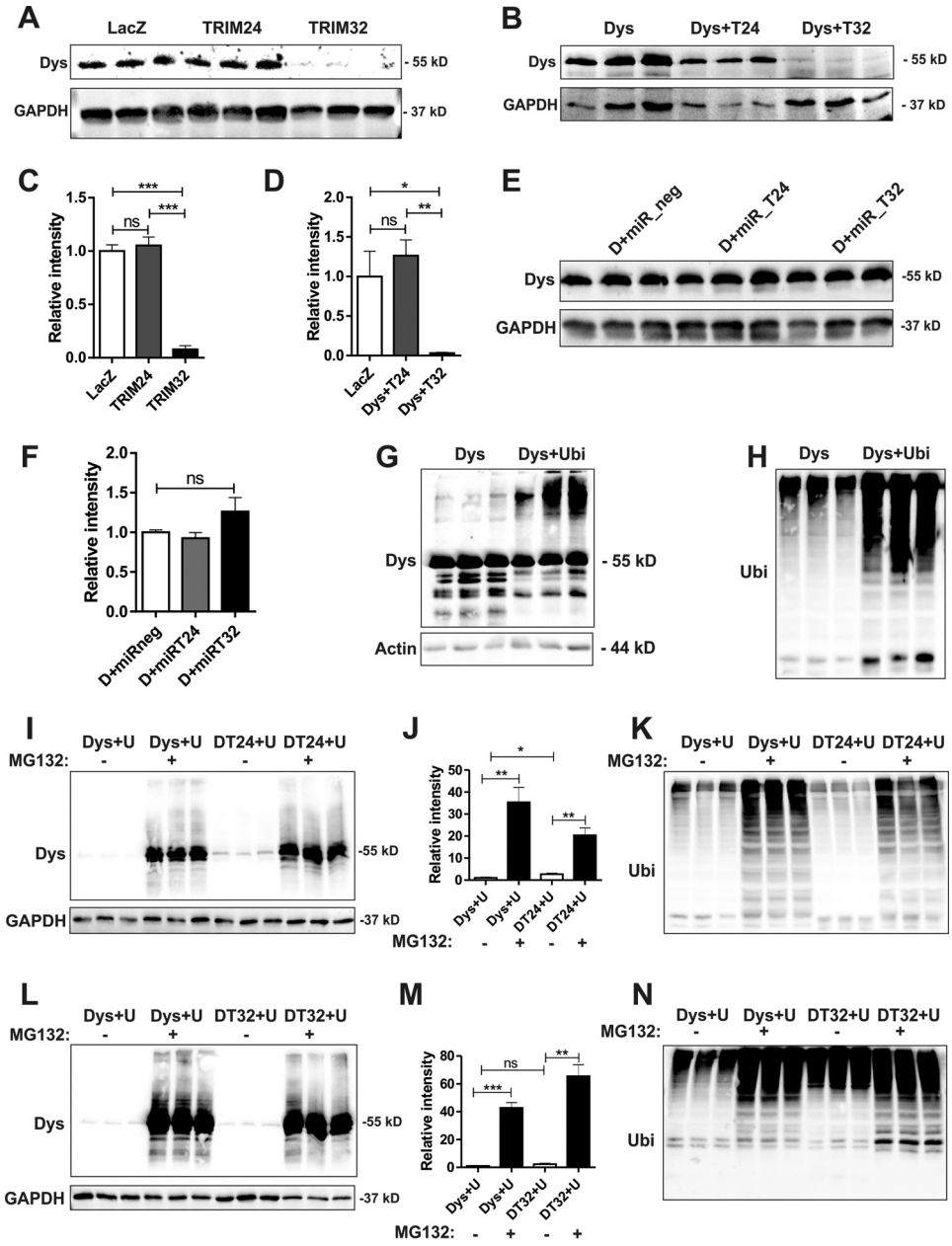

Figure 3. TRIM24 and TRIM32 antagonistically regulate dysbindin protein levels in NRVCMs. *A–D*, effect of adenovirus-mediated overexpression of TRIM24 (Ad-TRIM24, 100 ifu), and TRIM32 (Ad-TRIM32, 100 ifu) on endogenous (*A*) or overexpressed (*B*) (Ad-dysbindin, 50 ifu) dysbindin protein level indicates that TRIM24 does not, whereas TRIM32 does actively degrade dysbindin; respective densitometry data are presented as *graphs* in *C* and *D*. *E*, infection with synthetic microRNAs targeting either TRIM24 or TRIM32 did not alter dysbindin protein levels (densitometry in *F*). $n = 3$. *G*, overexpression of ubiquitin in the presence of dysbindin led to polyubiquitination of dysbindin as confirmed by the appearance of high molecular weight bands in *lanes 4–6* (ubiquitin overexpression is shown in *H*). *I*, effect of ubiquitin and UPS inhibitor MG132 on dysbindin protein levels when co-expressed with TRIM24; respective densitometry analysis presented in *graph J* clearly shows that TRIM24 partially restricted dysbindin degradation due to ubiquitin, whereas MG132 completely prevented dysbindin degradation suggesting direct involvement of the UPS system. *K*, ubiquitin immunoblot also indicates that the presence of TRIM24 reduces ubiquitin-driven polyubiquitination. Similarly, the presence of MG132 also attenuated the dysbindin degradation due to TRIM32 (*L* and *M*); nevertheless, in contrast to TRIM24, TRIM32 accelerated the polyubiquitination of cardiomyocyte proteins when co-expressed with ubiquitin (*N*). Statistical significance was determined using two-tailed Student's *t* test. *Error bars* show means ± S.E. *, $p < 0.05$; **, $p < 0.01$; ***, $p < 0.001$; *ns*, non-significant. *D* and *Dys*, dysbindin; *T24*, TRIM24; T32, TRIM32; *U* and *Ubi*, ubiquitin.

sion on NRVCMs was evident as predicted, and TRIM24 expression also exerted a similar effect (Fig. 5, *A* and *B*). In contrast, TRIM32 markedly reduced cell size when compared with cardiomyocytes expressing dysbindin or TRIM24 (Fig. 5, *A* and *B*). Furthermore, to our surprise, the total cell number of cultured NRVCMs was remarkably reduced in the presence of overexpressed TRIM32 (Fig. 5, *A* and *B*). This led us to further investigate the potential cause of this effect. Of note, dysbindin has previously been shown to play a supportive role in cell viability and proliferation in neurons (42, 43). Thus, we hypothesized that these effects are suppressed by TRIM32 by virtue of dysbindin degradation. To determine cell viability, we performed MTT assays. Cardiomyocyte survival indeed showed inverse relation with the expression of TRIM32 but not with dysbindin and TRIM24 expression (Fig. 5*C*). To visually confirm this negative effect of TRIM32 on cell viability and apopto-

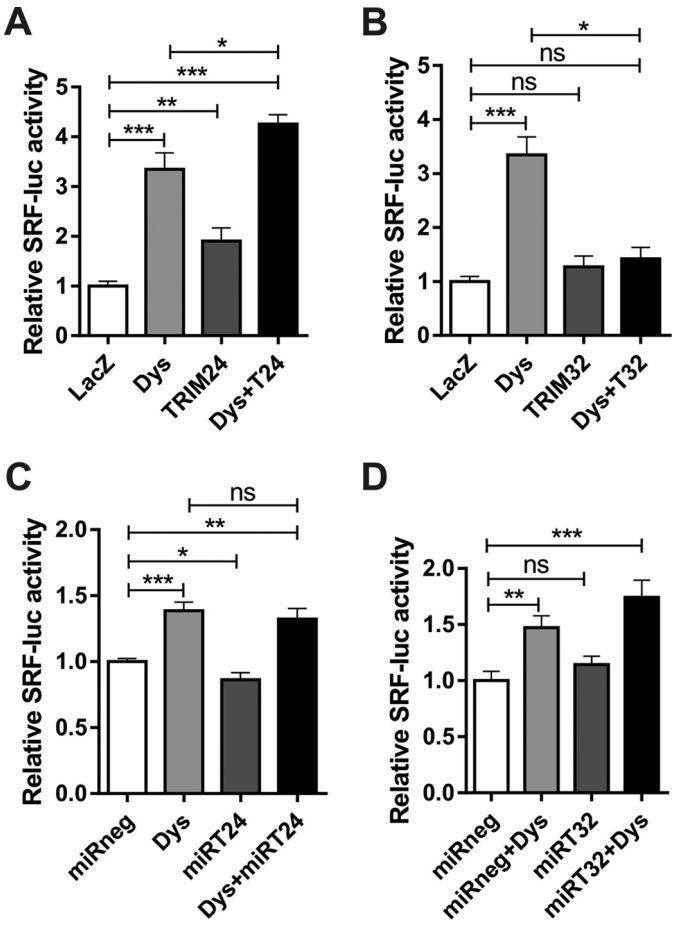

Figure 4. TRIM24 and TRIM32 antagonistically regulate SRF activity in NRVCMs. Effect of TRIM24 (*A*) and TRIM32 (*B*) on dysbindin-mediated luciferase activity determined by SRF-RE firefly luciferase reporter assay in NRVCMs. Adenoviruses expressing dysbindin (Ad-dysbindin, 50 ifu), TRIM24 (Ad-TRIM24, 100 ifu), TRIM32 (Ad-TRIM32, 100 ifu), SRF-RE reporter-based firefly luciferase (Ad-SRF-luc, 20 ifu), and *Renilla* luciferase (Ad-, 5 ifu, control) were used for infection in NRVCMs. Adenovirus expressing β-galactosidase (Ad-LacZ) was used as control or to maintain equal quantity of virus used for infection. Data shown are means of three independent experiments, $n = 6$. Synthetic microRNA specific for TRIM24 (*miRT24*) (*C*) or TRIM32 (*miRT32*) (*D*) was used for knockdown of endogenous TRIMs in NRVCMs to determine its effect on dysbindin-mediated SRF signaling by luciferase assay. Synthetic microRNA not targeting any transcript (*miRneg*) was used as a negative control. Data shown are means of two independent experiments performed in hexaplicate. Statistical significance was determined using two-tailed Student's *t* test. *Error bars* show means ± S.E. *, $p < 0.05$; **, $p < 0.01$; ***, $p < 0.001$; *ns,* non-significant. *Dys*, dysbindin; *T24,* TRIM24; *T32,* TRIM32; *miRT24*, microRNA-TRIM24; *miRT32,* microRNA-TRIM32.

sis, we also performed TUNEL assays and immunostainings with cleaved caspase-3 or propidium iodide (PI), a DNA intercalating stain that is excluded from membrane permeability in viable cells, thus commonly used to identify dead cells in a population. Again, the detrimental effect of TRIM32 on cell survival was consistent with TUNEL/caspase-3/PI staining, with the percentage of apoptotic cells surging up by 10%, when compared with the control cells expressing β-galactosidase (Figs. 5, *D*–*G*, and supplemental Fig. S4, *A* and *B*), implying presumable induction of apoptosis in NRVCMs. TUNEL-positive cells were reduced when dysbindin was overexpressed compared with the control cells (Fig. 5, *D* and *E*), although cleaved caspase-3 or PI-positive cells remained unchanged (Figs. 5, *F* and *G*, and supplemental Fig. S4, *A* and *B*). Notably, however, TRIM24 overexpression alone did not have any effect on cell viability or apoptosis (Figs. 5, *D*–*G*, and supplemental Fig. S4, *A* and *B*). These data indicate that TRIM32 is a strong modulator of cell viability and apoptosis in NRVCMs.

TRIM32 induces apoptosis in cardiomyocytes via caspase-3 and caspase-7 activation

Next, we wanted to ascertain the underlying mechanism how TRIM32 induces apoptosis. Caspases are known to be markers and mediators of apoptosis, initiating and executing programmed cell death (44). To investigate whether TRIM32 induces apoptosis via caspases, we determined the effect of dysbindin, TRIM24, and TRIM32 expression on caspase activation by immunoblotting. As anticipated, TRIM32 up-regulation in NRVCMs displayed strong appearance of cleaved fragments around 18 kDa for both caspase-3 (Fig. 6, *A* and *B*) and caspase-7 (Fig. 6, *C* and *D*), compared with the respective control groups. Caspase-3 is a known negative regulator of X-linked inhibitor of apoptosis (XIAP) (45) and exerts a positive influence on p53 expression (46), a well known carcinogenic marker that induces apoptosis in cancer cells. Moreover, XIAP is also a direct target of TRIM32 (47), and both TRIM24/32 have a known link with p53 in other cell types (35, 48, 49). In line with these findings, TRIM32 expression significantly decreased XIAP protein levels (Fig. 6, *E* and *F*) in cardiomyocytes. Furthermore, we found a significant reduction and a dramatic increase in p53 levels in the presence of dysbindin and TRIM32, respectively (Fig. 6, *G* and *H*). Overall, these findings indicate that TRIM32 robustly activates apoptosis in NRVCMs via caspase-3/XIAP signaling pathway.

TRIM24 protects dysbindin from degradation by TRIM32

Finally, we asked whether TRIM24 exhibits the potential to protect dysbindin degradation and downstream signaling via inhibition of TRIM32-mediated dysbindin degradation. Therefore, we repeated the cell size measurements, SRF signaling assays, and assessment of dysbindin protein levels in a set of experimental conditions where dysbindin was co-expressed with both TRIM24 and TRIM32 simultaneously. Of note, the negative effects of TRIM32 were significantly blunted by TRIM24, resulting in a larger cell size and increased SRF-signaling activity (Fig. 7, *A*–*C*). Remarkably, in the presence of TRIM24, the potent effect of TRIM32 on dysbindin degradation at the protein level is abrogated (Fig. 7, *D* and *E*). Thus, TRIM24 effectively counteracts TRIM32-driven dysbindin degradation with subsequent effects on cardiomyocyte growth and SRF signaling.

Discussion

The physiological role of dysbindin in the brain and its association with the psychiatric disorder schizophrenia is well established and has been shown in a series of research studies *in vitro*, in animal models, and in humans (50, 51). However, little is known about the role and regulation of this highly conserved and ubiquitously expressed protein in other cell types. Previously, our group reported dysbindin to be pro-hypertrophic and an SRF-signaling activator in neonatal rat cardiomyocytes

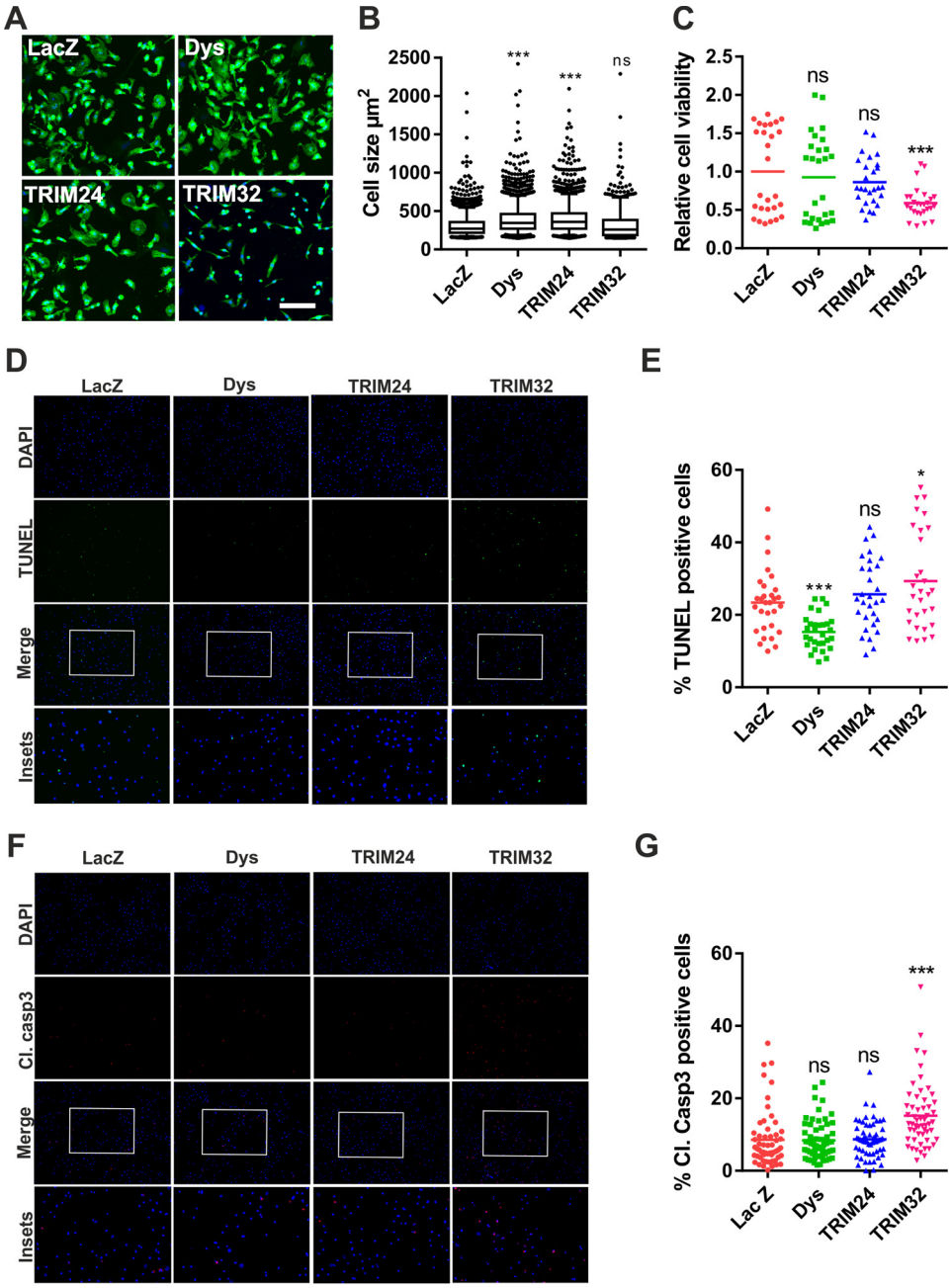

Figure 5. TRIM32 adversely affects cell viability and hypertrophy. *A,* representative images for cell-size analysis. NRVCMs were cultured on coverslips in triplicate, infected with adenovirus expressing LacZ (Ad-LacZ, control), dysbindin (Ad-dysbindin, 50 ifu), TRIM24 (Ad-TRIM24, 100 ifu), and TRIM32 (Ad-TRIM32, 100 ifu) for 72 h, and immunostained with α-actinin. Nuclei were stained with DAPI. Cell size analysis was performed on images taken with Keyence fluorescence microscope. *B,* cell surface area of the respective datasets was measured from randomly selected cells from three independent coverslips using MacroCellCount analyzer from BZ-II software. The experiment was repeated three times in triplicate. *C,* MTT assay for cell viability. Cultured NRVCMs were infected with adenovirus expressing dysbindin (Ad-dysbindin, 50 ifu), TRIM24 (Ad-TRIM24, 100 ifu), TRIM32 (Ad-TRIM32, 100 ifu) in serum-free media for 72 h. Adenovirus expressing β-galactosidase (Ad-LacZ) was used as control. After the incubation period, MTT-labeling reagent was added, and cells were incubated for 4 h in a humidified atmosphere. Subsequently, cells were subjected to overnight incubation with solubilization solution. Spectrophotometric absorbance was measured using Tecan ELISA reader. Data shown are means of three independent experiments performed in hexaplicates. *D* and *F*, representative images for TUNEL and cleaved caspase-3 staining in NRVCMs. After adenovirus infection for 72 h as mentioned above, NRVCMs underwent TUNEL staining (*D*) and immunostaining with cleaved caspase-3 (*F*). DAPI was used as nuclear stain for total nuclei. Respective analysis for percentage of TUNEL-positive (*E*) and cleaved caspase-3-positive (*G*) was performed with images taken from Keyence microscope. Nuclei count was performed with MacroCellCount analyzer. Data shown are means of two independent experiments performed in hexaplicates with >500 cells per condition. Statistical significance was determined using two-tailed Student's *t* test. *Error bars* show mean or means ± S.E. *, $p < 0.05$; ***, $p < 0.001$; *ns*, non-significant. *Scale bar* (shown with a white line), 100 μm. *Dys,* dysbindin; *Cl,* cleaved; *Casp3*, caspase-3.

(8). To further study the molecular function of dysbindin and to determine its binding partners in cardiomyocytes, we devised a yeast two-hybrid screen using dysbindin as bait against the human cardiac cDNA library. This screen resulted in the identification of TRIM24 as a new putative binding partner, in addition to RhoA and others. Here, we show that TRIM32, a previously reported E3 ubiquitin ligase of dysbindin, targets its degradation in cardiac muscle cells. Counterintuitively, TRIM24

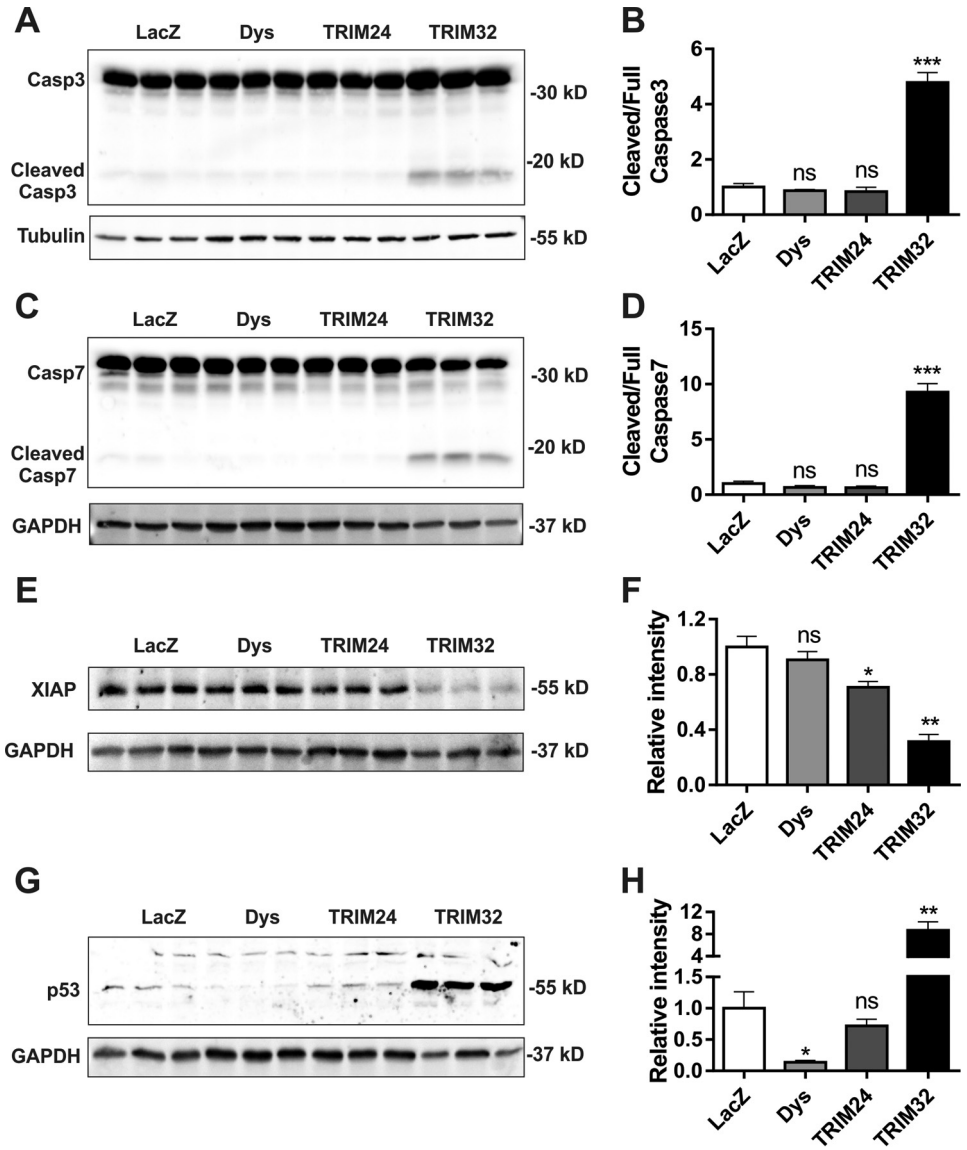

Figure 6. TRIM32 induces apoptosis in cardiomyocytes via caspase-3 and caspase-7 activations. *A* and *C,* immunoblots showing expression of apoptotic markers, caspase-3 and caspase-7, and their cleaved fragments (~18 kDa), respectively, in NRVCMs infected with adenovirus overexpressing dysbindin (Ad-dysbindin), TRIM24 (Ad-TRIM24), and TRIM32 (Ad-TRIM32). *B* and *D,* densitometric analysis for caspase-3 and caspase-7, cleaved fragment was performed by taking their respective uncleaved fragments as control. $n = 3$. *E,* immunoblot showing the expression of cellular apoptotic inhibitor protein XIAP and its densitometry analysis presented in a *bar graph* (*F*) with GAPDH as a loading control. *G,* immunoblot showing the expression of cellular apoptotic inducer in cancerous cells, p53, and its densitometry analysis presented in a *bar graph* (*H*) with GAPDH as a loading control. Statistical significance was determined using two-tailed Student's *t* test. *Error bars* show means ± S.E. *, $p < 0.05$; **, $p < 0.01$; ***, $p < 0.001$; *ns,* non-significant. *Casp3*, caspase-3; *Casp7,* caspase-7; *Dys,* dysbindin; *p53,* tumor protein 53; *XIAP,* X-linked inhibitor of apoptosis.

protects dysbindin from degradation. Furthermore, TRIM24 enhanced dysbindin function, its role in cellular hypertrophy, and SRF activation in cardiomyocytes, whereas TRIM32 attenuated these effects. Moreover, our studies indicate an anti-proliferative and pro-apoptotic role of TRIM32 in cardiomyocytes. In this study, we thus identified a new mechanism of post-transcriptional control of dysbindin levels mediated by these TRIM proteins.

Our study not only ascertains the interaction between dysbindin-TRIM32, but it also provides mechanistic insights into this interaction and downstream effects in cultured cardiomyocytes. TRIM32 is a ubiquitously expressed E3 ubiquitin ligase that is localized to the Z-line in skeletal muscle and has been shown to target desmin, actin, myosin, c-Myc, NDRG2, etc., in addition to dysbindin (30, 52–54). TRIM32 is necessary for muscle regeneration, myoblast proliferation, and differentiation (28, 30, 52–57) and has also been implicated in skeletal muscle atrophy (52). Here, we show that TRIM32 is significantly down-regulated in mouse models of hypertrophy caused by either infusion of PE or transverse aortic constriction and also in DCM and HCM patients, although it is not altered in the CnA-tg or MLP-ko mouse hearts. Interestingly, we observed an inconsistent low molecular weight protein band right below the expected TRIM32 band in the mouse hearts, which was highly up-regulated after TAC and in CnA-tg mouse hearts. We hypothesize that this additional band might represent a yet uncharacterized TRIM32 isoform that gets up-regulated due to the hypertrophic stress.

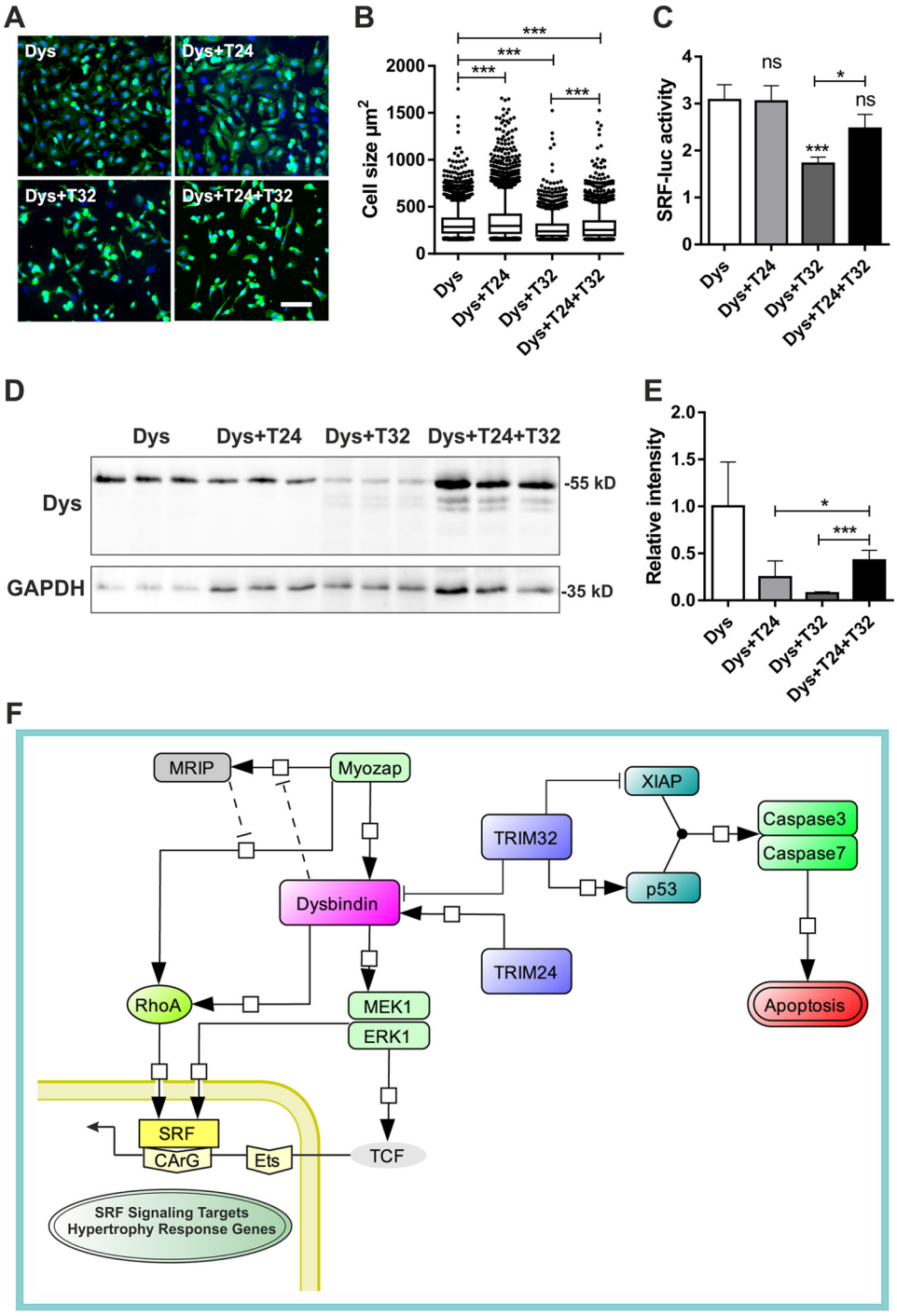

Figure 7. TRIM24 protects dysbindin from degradation by TRIM32. *A,* representative images for cell-size analysis. NRVCMs were cultured on coverslips in triplicate, infected with adenovirus expressing β-galactosidase (Ad-LacZ, control), dysbindin (Ad-dysbindin, 50 ifu), TRIM24 (Ad-TRIM24, 100 ifu), and TRIM32 (Ad-TRIM32, 100 ifu) for 72 h, and immunostained with α-actinin. Nuclei were stained with DAPI. Images were taken with Keyence fluorescence microscope. *B,* cell surface area of the respective datasets was measured from randomly selected cells from three independent coverslips using MacroCellCount analyzer from BZ-II software. The experiment was repeated three times in triplicate. *C,* effect of TRIM24 and TRIM32 in different combinations with dysbindin on SRF luciferase activity determined by SRF-RE firefly luciferase reporter assay in NRVCMs. Adenoviruses expressing dysbindin (Ad-dysbindin, 50 ifu), TRIM24 (Ad-TRIM24, 100 ifu), TRIM32 (Ad-TRIM32, 100 ifu), SRF-RE reporter-based firefly luciferase (Ad-SRF-luc, 20 ifu), and *Renilla* luciferase (Ad-*Renilla*, 5 ifu, control) were used for infection in NRVCMs. Data shown are means of three independent experiments performed in hexaplicate. *D,* immunoblot showing dysbindin expression in protein isolated from NRVCMs overexpressing dysbindin in combination with TRIM24 and/or TRIM32; its densitometry analysis is depicted by a *bar graph* in *E*. *F,* pictorial representation of the effects of TRIM24/32 on dysbindin and downstream signaling in cardiomyocytes. Dysbindin activates SRF signaling through direct interaction with Myozap and RhoA, consequently leading to induction of SRF-responsive genes and hypertrophy. Based on the data from this study, we propose that TRIM24 protects and promotes dysbindin-mediated hypertrophy and SRF signaling, whereas TRIM32 by virtue of dysbindin degradation inhibits hypertrophy and SRF signaling. TRIM32 also induces apoptosis via activation of p53, caspase-3/-7, and inhibition of XIAP in cardiomyocytes. Statistical significance was determined using two-tailed Student's *t* test. *Error bars* show means ± S.E. *, $p < 0.05$; ***, $p < 0.001$; *ns,* non-significant. *Scale bar* (shown with a *white line*), 100 μm.

While this work was in preparation, Chen *et al.* (31) provided a first hint toward a potential role for TRIM32 in the pathophysiology of the heart: Through gain- and loss-of-function approaches, they showed that TRIM32 protects the heart against pathological hypertrophy due to biomechanical stress (induced by transverse aortic constriction) or angiotensin II (31). Our data are in line with these findings and further provide a potential molecular mechanism to this phenomenon, as we show that TRIM32 restricts the pro-hypertrophic effects of dysbindin. Furthermore, we found that overexpression of TRIM32 is anti-proliferative and pro-apoptotic through the activation of caspase-3 and caspase-7. Activation of caspase-3 leads to inactivation of XIAP and activation of p53 (45, 46). To the contrary, as the name suggests, XIAP regulates apoptosis by inhibiting caspase-3 and -7 (58, 59). Notably, both XIAP and p53 are targets of TRIM32, whereas TRIM32 is reported to antagonize XIAP and is a negative regulator of p53 (47, 48). However, in this study, we report a rather strong up-regulation of p53 and down-regulation of XIAP when TRIM32 is overexpressed in cardiomyocytes suggesting a tissue-specific effect of TRIM32. Taken together, activation of p53/caspase-3/-7 and simultaneous inhibition of XIAP strongly contribute to the robust induction of apoptosis due to TRIM32 expression. Complementing our data, Hillje *et al.* (60) earlier showed that TRIM32 deficiency leads to increased proliferation and reduced apoptosis in neurons. In cancerous cells, however, TRIM32 is up-regulated and promotes tumorigenesis (48). In the heart, we speculate that the observed down-regulation of TRIM32 might be required for the development of (pathological) hypertrophy. It will thus be interesting to study this question *in vivo*, *e.g.* by restoring TRIM32 levels and assessing whether hypertrophy/heart failure still occurs. Nevertheless, the parallel effects of TRIM32 on cell survival might obscure the data, as TRIM32 could promote heart failure due to increased cell death even though hypertrophy is inhibited. Answering this question will be imperative before considering TRIM32 as a therapeutic target in pathological cardiac hypertrophy as proposed by Chen *et al.* (31).

Interestingly, we identified TRIM24, another TRIM family protein, as a new binding partner of dysbindin by a yeast two-hybrid screen from a cardiac cDNA library, which was further validated by co-immunoprecipitation in NRVCMs. TRIM24 was originally identified as transcriptional intermediary factor-1α (TIF-1α), a ligand-dependent co-repressor of retinoic acid receptor-α expression (61). Moreover, it is aberrantly expressed in human breast cancers and correlates with poor survival (39). The tissue distribution pattern of TRIM24/32 indicates that TRIM24 is expressed at higher levels than TRIM32 in the heart; however, to the best of our knowledge, no cardiac role for TRIM24 has yet been established. In contrast to TRIM32, TRIM24 was strongly up-regulated in mouse heart after PE infusion and in the hearts of human patients suffering from either DCM or HCM suggesting possible differential cardiac function for TRIM24 and TRIM32. It should also be noted that although TRIM24/32 share similar N-terminal RBCC domains, they carry distinct C-terminal motifs and hence are categorized into different subgroups (TRIM24 in subgroup VI and TRIM32 in subgroup VII (16)). It is therefore not surprising if two TRIMs exhibit contrasting effects in the same tissue for a given substrate, in this case, dysbindin. Although TRIM32 led to a strong reduction in dysbindin protein levels, TRIM24 rather protected TRIM32-mediated degradation of dysbindin. It was previously shown that TRIM32 interacts with dysbindin through its coiled-coil domain (30). Through mapping and co-immunoprecipitation experiments, we have also identified the coiled-coil domain of dysbindin to be the minimal domain required for its interaction with TRIM24. Hence, our data suggest that TRIM24 may inhibit the effects of TRIM32 through competitive binding. Moreover, by virtue of either protection or degradation of dysbindin levels in cardiomyocytes, the yin and yang function of TRIM24 and TRIM32 also regulates the pro-hypertrophic and SRF-activating effects of dysbindin, respectively.

Taken together, we here provide a novel mechanism of post-translational regulation of dysbindin in cardiomyocytes via its interaction partners TRIM24/32. This study also implies TRIM32 as a strong inducer of apoptosis in cardiomyocytes via concordant activation of p53 and caspase-3/-7 and inhibition of XIAP. Findings from this study and the known cardiac function of dysbindin from our previous work are summarized in a model cartoon (Fig. 7*F*).

In summary, this is the first report to show a cardiac role for TRIM24 in general and a protective role for dysbindin in particular. Moreover, the opposing effects of two TRIM proteins for a single target provide a novel pathway of post-translational regulation of dysbindin in cardiomyocytes. The association of dysbindin/TRIM24/32 with SRF signaling also makes this interaction interesting in the context of hypertrophy. Also, the strong apoptotic effects of TRIM32 are notable and might have wider implications in cardiac disease states. Finally, the differential expression of both TRIM24/32 in mouse models of biomechanical and biochemical hypertrophy and human patients suffering from DCM/HCM suggests a possible direct/indirect involvement of these TRIMs in cardiac pathophysiology, which needs future attention to decipher the underlying mechanisms. In broader terms, this study provides an initial characterization of two members of the TRIM family E3-ubiquitin ligases expressed in the heart, which need to be further explored for their *in vivo* and pathophysiological relevance.

Experimental procedures

Cloning of TRIM24 and TRIM32

Expression constructs for dysbindin and various dysbindin fragments were generated as described in Rangrez *et al.* (8). The plasmid for TRIM24 expression vector was a generous gift from Dr. Barton, University of Texas, Houston. TRIM32 was cloned from rat heart cDNA using primers 5′-GCTGGCACCATGGCTGCGGCTGCAGCA-3′ and 3′-GCTGGGTCGCCCTAAGGGGTAGAGTATCT-5′ in pDonR221 gateway cloning vector by following the manufacturer's instructions (Thermo Fisher Scientific). Knockdown of TRIM24 and TRIM32 was achieved by cloning the respective synthetic microRNAs using BLOCK-iT^{TM} polymerase II miR RNAi Expression vector kit and Gateway cloning system (Thermo Fisher Scientific).

Generation of recombinant adenoviruses and recombinant protein expression plasmids

Adenoviruses encoding full-length mouse dysbindin, human TRIM24, and rat TRIM32 cDNA and other necessary constructs (SRF-RE-luciferase, *Renilla* luciferase) were generated using the ViraPower adenoviral kit (Thermo Fisher Scientific) following the manufacturer's guidelines. In brief, previously cloned cDNA in pDonR221 vector was transferred into the pAd/CMV/V5-DEST destination vector. These constructs were then digested with PacI restriction enzyme and transfected into HEK293A cells to produce respective protein-expressing adenoviruses. Titration for the viruses was performed by staining virus-infected HEK293A cells with fluorescent anti-Hexon antibody. A β-galactosidase-V5-encoding adenovirus (Ad-LacZ; Thermo Fisher Scientific) served as a control. Similarly, for the generation of expression plasmids, the respective genes cloned into pDonR221 vector were transferred into pDest40 or pcDNA3.1 Gateway expression vectors, respectively, for transfection in mammalian cell lines.

Antibodies

Antibodies used for various experiments in this study were as follows: actin, goat polyclonal (1:3000; Santa Cruz Biotechnology), α-actinin, mouse monoclonal (1:200; Sigma); α-actinin, rabbit polyclonal (1:400; Abcam); α-tubulin, mouse monoclonal (1:8,000; Sigma); caspase-3, rabbit polyclonal (1:1,000; Cell Signaling Technology); cleaved caspase-3, rabbit monoclonal (1:400; Cell Signaling Technology); caspase-7, rabbit polyclonal (1:1,000; Cell Signaling Technology); dysbindin, mouse monoclonal (1:500, Santa Cruz Biotechnology); FLAG tag, mouse monoclonal (1:500; Sigma); GAPDH (1:20,000; Sigma); p53, mouse monoclonal (1:1,000, Novus Biologicals); TRIM24, rabbit polyclonal (1:1,000; Proteintech); TRIM32, rabbit polyclonal (1:500, Sigma); ubiquitin, mouse monoclonal (1:1,000; Millipore Upstate); V5 tag, mouse monoclonal (1:500; Biozol); and XIAP, rabbit polyclonal (1:1,000; Cell Signaling Technology).

Isolation of NRVCMs

NRVCMs were prepared as described previously (8). In brief, for isolation of NRVCMs, left ventricles from 1–2-day old Wistar rats (Charles River) were harvested and chopped in buffer B containing 120 mmol/liter NaCl, 20 mmol/liter Hepes, 8 mmol/liter NaH_2PO_4, 6 mmol/liter glucose, 5 mmol/liter KCl, and 0.8 mmol/liter $MgSO_4$, pH 7.4. For the release of individual cardiomyocytes from chopped tissue mass, five to six enzymatic digestion steps were performed with 0.6 mg/ml pancreatin (Sigma) at 37 °C and 0.5 mg/ml collagenase type II (Worthington) in sterile buffer B. Cell suspension was then passed through a cell strainer followed by the addition of newborn calf serum to stop enzymatic digestion. Cardiomyocytes were separated from fibroblasts using a Percoll gradient (GE Healthcare) centrifugation step and cultured in DMEM containing 10% fetal calf serum (FCS), 2 mM penicillin/streptomycin, and L-glutamine (PAA Laboratories). Adenovirus infection in DMEM supplemented with penicillin/streptomycin and L-glutamine but lacking FCS was performed 24 h post-harvest.

Co-IP in HEK293A cells

HEK293A cells were maintained in DMEM containing 4% FCS, 2 mM L-glutamine, and penicillin/streptomycin. Dysbindin was cloned with the C-terminal V5 tag, whereas both TRIM24 and TRIM32 were cloned with the N-terminal FLAG tag. For establishing interaction between dysbindin and TRIM proteins, HEK293A cells (2.5×10^6) were co-transfected with 10 μg each of TRIM expression plasmids with or without dysbindin using Lipofectamine 2000 (Life Technologies, Inc.). Empty vector pCGN-expressing HA tag was used as a negative control. 48 h after transfection with an intermittent media change at 24-h intervals, cells were washed with PBS, pelleted down, and resuspended in buffer A (50 mM Tris, 150 mM NaCl, 1% Nonidet P-40, 0.5% sodium deoxycholate, and 0.2% SDS) supplemented with phosphatase and protease inhibitor mixtures (Complete; Roche Applied Science). Cells were lysed by three successive freeze-thaw cycles followed by centrifugation at 18,000 × *g* at 4 °C for 20 min. The supernatant containing cellular proteins was used for immunoprecipitation using anti-V5 or anti-FLAG affinity gels in two separate setups following the manufacturer's guidelines. In brief, 1 mg of protein in a total volume of 1 ml of lysis buffer was applied to 50 μl of equilibrated beads, and V5- and FLAG-tagged proteins were then allowed to bind to the respective antibody on the beads for ~4 h at 4 °C atop a rotating shaker. Protein lysate was removed carefully after centrifugation at 8,000 × *g*, and magnetic beads were washed 4–5 times with lysis buffer. Precipitated proteins from the beads were eluted with 50 μl of Laemmli sample buffer. 10 μl of this eluted protein was immunoblotted with SDS-PAGE followed by transfer to nitrocellulose membranes and developed against anti-FLAG or anti-V5 antibodies for checking two-way interactions between dysbindin and TRIM proteins. All the co-IP experiments were performed twice.

Co-IP in NRVCMs

Cultured NRVCMs (6×10^6) were co-infected with adenoviruses for HA-tagged dysbindin (Ad-HA-dysbindin, 50 ifu), TRIM24 (Ad-TRIM24, 100 ifu), TRIM24 (Ad-TRIM24, 100 ifu), and TRIM32 (Ad-TRIM32, 100 ifu) in several setups in DMEM containing 2 mM penicillin/streptomycin and L-glutamine but lacking FCS. Adenovirus expressing β-galactosidase (Ad-LacZ) was used as negative control for all the co-IP experiments. 72 h after infection, cells were washed with PBS, pelleted, and resuspended in buffer A (50 mM Tris, 150 mM NaCl, 1% Nonidet P-40, 0.5% sodium deoxycholate, and 0.2% SDS) supplemented with phosphatase and protease inhibitor mixture (Complete; Roche Applied Science). Cells were lysed three times by freeze-thaw, and debris was removed by centrifugation. Supernatant-containing protein was used for the immunoprecipitation using anti-HA affinity gel (EZview Red; Sigma) following the manufacturer's guidelines. In brief, 1 mg of protein in a total volume of 1 ml of buffer A was applied to 50 μl of equilibrated beads, and HA-tagged proteins were allowed to bind to anti-HA antibody on the beads for ~4 h at 4 °C atop a rotating shaker. Protein lysate was removed carefully after centrifugation at 8,200 × *g*, and beads were washed for four to five times with lysis buffer. Precipitated proteins from the beads

were eluted with 50 μl of Laemmli sample buffer. 10–15 μl of this eluted protein was immunoblotted with SDS-PAGE followed by transfer to nitrocellulose membranes against various antisera, including TRIM24, TRIM32, dysbindin, HA, etc. All co-IP experiments were performed at least twice.

Confocal immunofluorescence microscopy

Co-localization studies of dysbindin with TRIM24 and TRIM32 were carried out in NRVCM. NRVCMs were seeded in a 12-well plate on collagen-coated coverslips. Following the adenovirus infection and incubation phase, NRVCMs were fixed with 4% paraformaldehyde for 10 min, permeabilized, and blocked with 0.1% Triton X-100 in 2.5% BSA in phosphate-buffered saline (PBS) for 1 h at room temperature. Cells were then incubated for 1 h with primary antibodies using the following dilutions: monoclonal mouse anti-dysbindin (1:100; Santa Cruz Biotechnology), monoclonal mouse anti-α-actinin (1:200; Sigma), polyclonal rabbit anti-α-actinin (1:400; Abcam), polyclonal rabbit anti-TRIM24 (1:200; Acris), and polyclonal rabbit anti-TRIM32 (1:200, Sigma) for co-localization. Respective secondary antibodies conjugated to either Alexa Fluor-488 (AF488), Alexa Fluor-546 (AF546), or Alexa Fluor-647 (Thermo Fisher Scientific) were incubated for 1 h at a dilution of 1:200 in 2.5% BSA in PBS, along with nuclear stain DAPI. FluorPreserve reagent (Merck Millipore) was used as mounting medium. Confocal images were taken with a Zeiss LSM800 laser-scanning microscope with a Plan-Apochromat $\times$40/1.4 oil differential interference contrast (UV)-visible IR objective at room temperature. Image pixel size was set to optimal for individual acquisitions. Pinhole was adjusted to 1 airy unit or less for each individual laser line. AF546 and DAPI channels were acquired via GaAsP-Pmt detectors and AF488 channel with a Multialkali-Pmt detector with gain settings between 600 and 700 V. The laser power for excitation ranged from 0.2 to 0.8%. Cropped regions from the overviews are not digital magnifications of the areas but newly acquired images.

Co-localization analysis

The co-localization analyses were carried out using the Zeiss co-localization method ZEN-blue software package. Individual cells from three different overview images were taken into the measurement to maintain co-localization coefficient calculation integrity. For setting the scatter plot boundaries and to automatically identify the threshold value to be used to identify background values, we utilized the method of Coste *et al.* (62), which was automatically implemented by the software. To assess the fraction of a protein that co-localizes with another protein, we utilized the Mander's co-localization coefficients (MCC) (63), which are metrics that are widely used in biological microscopy analyses and have been implemented in all biological image analysis software packages (64). MCC measures co-occurrence independent of signal proportionality and ranges from 0 to 1, where an MCC of 1 represents 100% co-localizations of the respective dyes.

TAC

TAC was performed in 8-week-old C57BL/N mice as described previously (6). Briefly, mice were anesthetized with combination of ketamine (120 mg/kg i.p.) and xylazine (15 mg/kg i.p.). The mice were then orally intubated with a 20-gauge tube and ventilated (Harvard Apparatus) at 120 breaths per min (0.2-ml tidal volume). The aortic constriction was performed via a lateral thoracotomy through the second intercostal space. A suture (Prolene 6-0) was placed around the transverse aorta between the brachiocephalic and left carotid artery. The suture was ligated against a 27-gauge needle. The needle was later removed leaving a discrete stenosis. The chest was sutured and the pneumothorax evacuated. Sham-operated animals underwent the same procedure except for ligation. Cardiac function was examined by echocardiography, and the animals were killed 2 weeks post-implantation to extract the heart and for downstream applications. All the animal experiments were approved and performed as per the guidelines of local ethical committee (Ministerium für Energiewende, Landwirtschaft, Umwelt and Ländliche Räume Schleswig-Holstein).

Human DCH and HCM heart samples

Left ventricular myocardial tissue was taken from explanted hearts of XX patients (HCM, $n = 4$; DCM, $n = 10$; NF, $n = 7$) with end-stage heart failure (New York Heart Association heart failure classification IV) undergoing heart transplantation. All procedures involving humans were performed in compliance with the ethical committee of the medical school of the Georg-August-University, Göttingen, Germany. The explanted hearts were acquired directly in the operating room during surgical procedures and immediately placed in pre-cooled cardioplegic solution (in mmol/liter: NaCl 110, KCl 16, $MgCl_2$ 16, $NaHCO_3$ 16, $CaCl_2$ 1.2, glucose 11). Myocardial samples for Western blot analysis were frozen in liquid nitrogen and stored at -80 °C immediately after excision.

Phenylephrine osmotic pump implantation

Osmotic mini-pumps filled with α-adrenergic agonist phenylephrine (25 μg/kg body weight/min) prepared in phosphate-buffered saline (PBS) with 1 mg/ml L-ascorbate (Sigma) were implanted subcutaneously in 8-week-old C57BL/N mice. Control group received the vehicle L-ascorbate in PBS. Cardiac function was examined by echocardiography, and the animals were killed 2 weeks post-implantation to extract the heart and for downstream applications.

SRF reporter gene assay

SRF reporter gene assays shown in this study were performed in NRVCMs as described previously (8). Briefly, cells were infected with several combinations of viruses expressing dysbindin (50 ifu), TRIM24 (100 ifu), TRIM32 (100 ifu), and LacZ (as control or a filler virus to maintain equal count of viruses) along with adenovirus Ad-SRF-RE-luciferase (20 ifu) carrying a firefly luciferase and Ad-*Renilla*-luciferase carrying (5 ifu) *Renilla* luciferase (for normalization of the measurements). For TRIM24 and TRIM32 knockdown experiments, NRVCMs were transfected with Ad-miRTRIM24 and Ad-miRTRIM32 where microRNA (Ad-miRneg) was used as control or filler in addition to adenovirus infection. Experiments were performed using a dual-luciferase reporter assay kit (Promega), according to the manufacturer's guidelines. Chemiluminescence was mea-

sured photometrically on an Infinite M200 PRO system (Tecan, Life Science). All the experiments were performed in quadruplicate or hexaplicate and repeated three times.

Immunofluorescence microscopy

Cell size measurements, TUNEL, cleaved caspase-3, and PI staining were studied in NRVCMs by immunofluorescence microscopy. Cell preparation and staining were performed as described above. Monoclonal mouse anti-α-actinin (1:200; Sigma) was used for cell size measurements, whereas polyclonal rabbit anti-cleaved caspase-3 (1:400, Cell Signaling Technology) antibody was used for activated caspase-3 staining. Respective secondary antibodies conjugated to either Alexa Fluor-488 or Alexa Fluor-546 (Thermo Fisher Scientific) were incubated for 1 h at a dilution of 1:200 in 2.5% BSA in PBS along with nuclear stain DAPI. FluorPreserve reagent (Merck Millipore) was used as mounting medium. Fluorescence micrographs were taken with Keyence fluorescence microscope BZ 9000, at $\times$10 objective (Plan Apochromat, NA: 0.45). Images were acquired using BZ-II viewer software (Keyence, version 2.1) using a built-in camera at room temperature. Images were processed and analyzed by BZ-II Analyzer (Keyence, version 2.1) as detailed below.

Cell surface area measurement using BZ-9000 microscope

Immunofluorescence pictures were taken using the BZ-9000 microscope. For each coverslip with fluorescence-stained cells, 10 pictures were taken at $\times$10 magnification (objective: CFI Plan Apochromat λ $\times$10; Nikon) with BZ-II Viewer (version 2.1). Images were further processed and analyzed using the BZ-II Analyzer (version 2.1). Cell size was measured using HybridCellCount software module (Keyence) with the fluorescence intensity single-extraction mode. First, fluorescence intensity thresholds were set for a reference picture. Thereafter, α-actinin whole-cell staining was set as the target area, and the DAPI-stained nuclei were then extracted from each target area to determine the number of nuclei per target area. Then MacroCellCount was performed, applying the settings from the reference picture to each picture from one set of experiments. Results were manually filtered for the following criteria: (*a*) 150-μm^2 $<$ target area in micrometers squared $<$2,500 μm^2 (size filter); (*b*) extraction from target area = 1 (one nucleus filter); and (*c*) area ratio 1 $<$30% (cell surface to nucleus ratio filter). Statistical analyses were performed using GraphPad Prism (version 5). Equal distribution of the data were tested by Shapiro-Wilk test. The samples were then compared by Student's *t* test. $n \geq 700$ (each condition, depending on the cell density).

MTT assay for cell viability

NRVCMs cultured in 24-well plates were infected with respective adenoviruses and incubated for 72 h. MTT labeling reagent (cell proliferation kit, MTT I, Roche Applied Science) was added at 10% concentration of total DMEM to each well. Plates were incubated for 4 h in a humidified atmosphere (37 °C, 5% CO_2). After this incubation phase, MTT solubilization solution (cell proliferation kit, MTT I, Roche Applied Science) was added to each well with a quantity of 10 times the initially added MTT labeling reagent and incubated overnight under the incubation conditions mentioned above. After complete solubilization of purple formazan crystals, spectrophotometric absorbance was measured using a microplate reader on an Infinite M200 PRO System (Tecan, Life Science). The percentage of viable cells was plotted relative to control. Samples were then compared by Student's *t* test. All the experiments were performed in hexaplicate or octaplicate and repeated three times.

TUNEL assay

NRVCMs were seeded in a 12-well plate on collagen-coated coverslips. Following the adenovirus infection and 72-h incubation phase, NRVCMs were fixed with 4% paraformaldehyde for 10 min, permeabilized/blocked with PBS containing 2.5% BSA and 0.1% Triton X-100 for 1 h at room temperature. An enzyme mixture was prepared by adding TUNEL mix into labeling solution at 1:10 ratio (*In situ*-Cell death detection kit, Roche Applied Science). Positive control was treated with DNase enzyme for 10 min, and the enzyme mixture for negative control lacking TUNEL mix. All coverslips were incubated at 37 °C for 1 h along with controls in their respective enzyme mixtures. Nuclear staining was performed with DAPI for 15 min after incubation phase and three washings with PBS. Coverslips were mounted with FluorPreserve reagent (Merck Millipore). Acquisition of fluorescent micrographs was performed as described earlier for cell size imaging. Images were further processed and analyzed using the BZ-II Analyzer (version 2.1). Processing was executed using HybridCellCount software module (Keyence) with the fluorescence intensity single extraction mode. First, fluorescence intensity thresholds were set for a reference picture. Thereafter, DAPI nuclear staining was set as the target stain, and the TUNEL-stained nuclei were then extracted from each target nuclei to determine the number of TUNEL/DAPI-stained nuclei per coverslip. Then, MacroCellCount was performed, applying the settings from the reference picture to overlying images from each set of experiments. Statistical analyses were performed using GraphPad Prism (version 5), and samples were compared by Student's *t* test, $n \geq 700$ (each condition, depending on the cell density).

Nuclei count for cleaved caspase-3 and PI staining

Immunostaining for cleaved caspase-3 was carried out as described under "Immunofluorescence microscopy." For PI staining, NRVCMs cultured on collagen-coated coverslips were treated with 1 mM PI diluted in PBS (1:2,000) for 5 min after a 72-h incubation period. Cells were then fixed on coverslips with cold methanol at -20 °C for 10 min and mounted using FluorPreserve reagent (Merck Millipore) along with DAPI. Fluorescence micrographs were taken at $\times$10 objective as explained above. Images were then analyzed with the BZ-II analyzer separately for DAPI and PI/caspase-3 by keeping off the extraction mode. The total number of nuclei were counted by HybridCellCount and plotted by taking the percentage of PI-stained or cleaved caspase-3-positive nuclei over DAPI-stained nuclei for individual coverslips. All these experiments are repeated twice in triplicate. The samples were then compared by Student's *t* test.

RNA isolation and qRT-PCR

Total RNA was isolated from NRVCMs, mouse heart (or other tissues), or human heart samples using lysis reagent (QIAzol; Qiagen) following the manufacturer's instructions. 1 μg of DNA-free total RNA was transcribed into cDNA using the first strand cDNA synthesis kit (SuperScript III; Life Technologies, Inc.). For qRT-PCR, the EXPRESS SYBR Green ER reagent (Life Technologies, Inc.) was used in a real-time PCR system (CFX96; Bio-Rad). Cycling conditions used for all the qRT-PCRs are 3 min at 95 °C followed by 40 cycles of 15 s at 95 °C and 45 s at 60 °C, a common step for annealing and extension at which step data were collected. Rpl32 or 18S ribosomal RNA genes were used as an internal standard for normalization (65). All experiments with NRVCMs were performed in triplicate and repeated three times.

Protein preparation and immunoblotting

NRVCMs were lysed by two to three freeze-thaw cycles in lysis buffer A containing 50 mM Tris, 150 mM NaCl, 1% Nonidet P-40, 0.5% sodium deoxycholate, and 0.2% SDS along with phosphatase inhibitor II, phosphatase inhibitor III, and protease inhibitor mixture (Roche Applied Science). Cell debris was removed by centrifugation, and protein concentration was determined photometrically by DC assay method (Bio-Rad). Protein from adult mouse and human hearts was harvested by homogenizing heart fragments along with Precellys ceramic beads (Peqlab) in lysis buffer A. Protein samples were resolved by 10% SDS-PAGE, transferred to a nitrocellulose membrane, and immunoblotted with the target-specific primary antibodies. The overnight application of primary antibodies was followed by incubation with a suitable HRP-coupled secondary antibody (1:10,000; Santa Cruz Biotechnology) or fluorescent antibody Alexa Fluor 546. Finally, visualization was achieved using a chemiluminescence kit (GE Healthcare) and was detected on an imaging system (FluorChem Q; Biozym). Quantitative densitometry was performed using ImageJ version 1.46 software (National Institutes of Health).

Statistical analyses

All results are shown as the means ± S.E. unless stated otherwise. Statistical analyses of the data were performed using two-tailed Student's *t* test. When necessary, two-way analysis of variance (followed by Student-Newman-Keuls post hoc tests when appropriate) was applied. p values of less than 0.05 were considered statistically significant.

Author contributions—A. Y. R. and N. F. devised the experimental strategy. A. Borlepawar conducted most of the experiments. D. F. designed and analyzed the Y2H study. L. C. generated and validated the expression constructs in NRVCMs and performed immunoprecipitation. A. Bernt performed confocal microscopy, analyzed the data, and prepared the respective images. S. S. obtained human DCM and non-failing heart samples with ethical permission and consent. A. Borlepawar and A. Y. R. analyzed the results and wrote the primary draft of the manuscript. N. F. wrote some part of the manuscript, and N. F., D. F., and A. Y. R. critically revised the manuscript. All authors approved final version of the manuscript.

Acknowledgments—Y2H screening was performed at the protein interaction unit of the Genomics and Proteomics Core Facility at German Cancer Research Center (Heidelberg, Germany). We thank Gabriele Brunke, Katharina Stiebeling, Vanessa Mangels, and Christin Tannert for their excellent technical assistance.

References

1. Molkentin, J. D., Lu, J. R., Antos, C. L., Markham, B., Richardson, J., Robbins, J., Grant, S. R., and Olson, E. N. (1998) A calcineurin-dependent transcriptional pathway for cardiac hypertrophy. *Cell* **93,** 215–228
2. Frey, N., and Olson, E. N. (2003) Cardiac hypertrophy: the good, the bad, and the ugly. *Annu. Rev. Physiol.* **65,** 45–79
3. Naga Prasad, S. V., Esposito, G., Mao, L., Koch, W. J., and Rockman, H. A. (2000) G$\beta\gamma$-Dependent phosphoinositide 3-kinase activation in hearts with *in vivo* pressure overload hypertrophy. *J. Biol. Chem.* **275,** 4693–4698
4. Sotiropoulos, A., Gineitis, D., Copeland, J., and Treisman, R. (1999) Signal-regulated activation of serum response factor is mediated by changes in actin dynamics. *Cell* **98,** 159–169
5. Frank, D., Rangrez, A. Y., Poyanmehr, R., Seeger, T. S., Kuhn, C., Eden, M., Stiebeling, K., Bernt, A., Grund, C., Franke, W. W., and Frey, N. (2014) Mice with cardiac-restricted overexpression of Myozap are sensitized to biomechanical stress and develop a protein-aggregate-associated cardiomyopathy. *J. Mol. Cell. Cardiol.* **72,** 196–207
6. Rangrez, A. Y., Eden, M., Poyanmehr, R., Kuhn, C., Stiebeling, K., Dierck, F., Bernt, A., Lüllmann-Rauch, R., Weiler, H., Kirchof, P., Frank, D., and Frey, N. (2016) Myozap deficiency promotes adverse cardiac remodeling via differential regulation of mitogen-activated protein kinase/serum-response factor and β-catenin/GSK-3β protein signaling. *J. Biol. Chem.* **291,** 4128–4143
7. Seeger, T. S., Frank, D., Rohr, C., Will, R., Just, S., Grund, C., Lyon, R., Luedde, M., Koegl, M., Sheikh, F., Rottbauer, W., Franke, W. W., Katus, H. A., Olson, E. N., and Frey, N. (2010) Myozap, a novel intercalated disc protein, activates serum response factor-dependent signaling and is required to maintain cardiac function *in vivo*. *Circ. Res.* **106,** 880–890
8. Rangrez, A. Y., Bernt, A., Poyanmehr, R., Harazin, V., Boomgaarden, I., Kuhn, C., Rohrbeck, A., Frank, D., and Frey, N. (2013) Dysbindin is a potent inducer of RhoA-SRF-mediated cardiomyocyte hypertrophy. *J. Cell Biol.* **203,** 643–656
9. Arnold, S. E., Talbot, K., and Hahn, C. G. (2005) Neurodevelopment, neuroplasticity, and new genes for schizophrenia. *Prog Brain Res.* **147,** 319–345
10. Fei, E., Ma, X., Zhu, C., Xue, T., Yan, J., Xu, Y., Zhou, J., and Wang, G. (2010) Nucleocytoplasmic shuttling of dysbindin-1, a schizophrenia-related protein, regulates synapsin I expression. *J. Biol. Chem.* **285,** 38630–38640
11. Fu, C., Chen, D., Chen, R., Hu, Q., and Wang, G. (2015) The schizophrenia-related protein dysbindin-1A is degraded and facilitates NF-κB activity in the nucleus. *PLoS One* **10,** e0132639
12. Ma, X., Fei, E., Fu, C., Ren, H., and Wang, G. (2011) Dysbindin-1, a schizophrenia-related protein, facilitates neurite outgrowth by promoting the transcriptional activity of p53. *Mol. Psychiatr.* **16,** 1105–1116
13. Owen, M. J., Williams, N. M., and O'Donovan, M. C. (2004) Dysbindin-1 and schizophrenia: from genetics to neuropathology. *J. Clin. Invest.* **113,** 1255–1257
14. James, L. C., Keeble, A. H., Khan, Z., Rhodes, D. A., and Trowsdale, J. (2007) Structural basis for PRYSPRY-mediated tripartite motif (TRIM) protein function. *Proc. Natl. Acad. Sci. U.S.A.* **104,** 6200–6205
15. Nisole, S., Stoye, J. P., and Saïb, A. (2005) TRIM family proteins: retroviral restriction and antiviral defence. *Nat. Rev. Microbiol.* **3,** 799–808
16. Ozato, K., Shin, D. M., Chang, T. H., and Morse, H. C., 3rd. (2008) TRIM family proteins and their emerging roles in innate immunity. *Nat. Rev. Immunol.* **8,** 849–860
17. Meroni, G., and Diez-Roux, G. (2005) TRIM/RBCC, a novel class of 'single protein RING finger' E3 ubiquitin ligases. *Bioessays* **27,** 1147–1157

18. Arya, R., Kedar, V., Hwang, J. R., McDonough, H., Li, H. H., Taylor, J., and Patterson, C. (2004) Muscle ring finger protein-1 inhibits PKCε activation and prevents cardiomyocyte hypertrophy. *J. Cell Biol.* **167,** 1147–1159
19. Kedar, V., McDonough, H., Arya, R., Li, H. H., Rockman, H. A., and Patterson, C. (2004) Muscle-specific RING finger 1 is a bona fide ubiquitin ligase that degrades cardiac troponin I. *Proc. Natl. Acad. Sci. U.S.A.* **101,** 18135–18140
20. Willis, M. S., Ike, C., Li, L., Wang, D. Z., Glass, D. J., and Patterson, C. (2007) Muscle ring finger 1, but not muscle ring finger 2, regulates cardiac hypertrophy *in vivo*. *Circ. Res.* **100,** 456–459
21. Fielitz, J., van Rooij, E., Spencer, J. A., Shelton, J. M., Latif, S., van der Nagel, R., Bezprozvannaya, S., de Windt, L., Richardson, J. A., Bassel-Duby, R., and Olson, E. N. (2007) Loss of muscle-specific RING-finger 3 predisposes the heart to cardiac rupture after myocardial infarction. *Proc. Natl. Acad. Sci. U.S.A.* **104,** 4377–4382
22. Fielitz, J., Kim, M. S., Shelton, J. M., Latif, S., Spencer, J. A., Glass, D. J., Richardson, J. A., Bassel-Duby, R., and Olson, E. N. (2007) Myosin accumulation and striated muscle myopathy result from the loss of muscle RING finger 1 and 3. *J. Clin. Invest.* **117,** 2486–2495
23. Willis, M. S., Schisler, J. C., Li, L., Rodríguez, J. E., Hilliard, E. G., Charles, P. C., and Patterson, C. (2009) Cardiac muscle ring finger-1 increases susceptibility to heart failure *in vivo*. *Circ. Res.* **105,** 80–88
24. Li, H. H., Du, J., Fan, Y. N., Zhang, M. L., Liu, D. P., Li, L., Lockyer, P., Kang, E. Y., Patterson, C., and Willis, M. S. (2011) The ubiquitin ligase MuRF1 protects against cardiac ischemia/reperfusion injury by its proteasome-dependent degradation of phospho-c-Jun. *Am. J. Pathol.* **178,** 1043–1058
25. Chen, S. N., Czernuszewicz, G., Tan, Y., Lombardi, R., Jin, J., Willerson, J. T., and Marian, A. J. (2012) Human molecular genetic and functional studies identify TRIM63, encoding muscle RING finger protein 1, as a novel gene for human hypertrophic cardiomyopathy. *Circ. Res.* **111,** 907–919
26. Su, M., Wang, J., Kang, L., Wang, Y., Zou, Y., Feng, X., Wang, D., Ahmad, F., Zhou, X., Hui, R., and Song, L. (2014) Rare variants in genes encoding MuRF1 and MuRF2 are modifiers of hypertrophic cardiomyopathy. *Int. J. Mol. Sci.* **15,** 9302–9313
27. Schlossarek, S., Frey, N., and Carrier, L. (2014) Ubiquitin-proteasome system and hereditary cardiomyopathies. *J Mol. Cell. Cardiol.* **71,** 25–31
28. Shieh, P. B., Kudryashova, E., and Spencer, M. J. (2011) Limb-girdle muscular dystrophy 2H and the role of TRIM32. *Handb. Clin. Neurol.* **101,** 125–133
29. Chiang, A. P., Beck, J. S., Yen, H. J., Tayeh, M. K., Scheetz, T. E., Swiderski, R. E., Nishimura, D. Y., Braun, T. A., Kim, K. Y., Huang, J., Elbedour, K., Carmi, R., Slusarski, D. C., Casavant, T. L., Stone, E. M., and Sheffield, V. C. (2006) Homozygosity mapping with SNP arrays identifies TRIM32 an E3 ubiquitin ligase, as a Bardet-Biedl syndrome gene (BBS11). *Proc. Natl. Acad. Sci. U.S.A.* **103,** 6287–6292
30. Locke, M., Tinsley, C. L., Benson, M. A., and Blake, D. J. (2009) TRIM32 is an E3 ubiquitin ligase for dysbindin. *Hum. Mol. Genet.* **18,** 2344–2358
31. Chen, L., Huang, J., Ji, Y., Zhang, X., Wang, P., Deng, K., Jiang, X., Ma, G., and Li, H. (2016) Tripartite motif 32 prevents pathological cardiac hypertrophy. *Clin. Sci.* **130,** 813–828
32. Jiang, S., Minter, L. C., Stratton, S. A., Yang, P., Abbas, H. A., Akdemir, Z. C., Pant, V., Post, S., Gagea, M., Lee, R. G., Lozano, G., and Barton, M. C. (2015) TRIM24 suppresses development of spontaneous hepatic lipid accumulation and hepatocellular carcinoma in mice. *J. Hepatol.* **62,** 371–379
33. Wang, J., Zhu, J., Dong, M., Yu, H., Dai, X., and Li, K. (2014) Knockdown of tripartite motif containing 24 by lentivirus suppresses cell growth and induces apoptosis in human colorectal cancer cells. *Oncol. Res.* **22,** 39–45
34. Xue, D., Zhang, X., Zhang, X., Liu, J., Li, N., Liu, C., Liu, Y., and Wang, P. (2015) Clinical significance and biological roles of TRIM24 in human bladder carcinoma. *Tumour Biol.* **36,** 6849–6855
35. Allton, K., Jain, A. K., Herz, H. M., Tsai, W. W., Jung, S. Y., Qin, J., Bergmann, A., Johnson, R. L., and Barton, M. C. (2009) Trim24 targets endogenous p53 for degradation. *Proc. Natl. Acad. Sci. U.S.A.* **106,** 11612–11616
36. Le Douarin, B., Nielsen, A. L., You, J., Chambon, P., and Losson, R. (1997) TIF1α: a chromatin-specific mediator for the ligand-dependent activation function AF-2 of nuclear receptors? *Biochem. Soc. Trans.* **25,** 605–612
37. Groner, A. C., Cato, L., de Tribolet-Hardy, J., Bernasocchi, T., Janouskova, H., Melchers, D., Houtman, R., Cato, A. C., Tschopp, P., Gu, L., Corsinotti, A., Zhong, Q., Fankhauser, C., Fritz, C., Poyet, C., *et al.* (2016) TRIM24 is an oncogenic transcriptional activator in prostate cancer. *Cancer Cell* **29,** 846–858
38. Thénot, S., Henriquet, C., Rochefort, H., and Cavaillès, V. (1997) Differential interaction of nuclear receptors with the putative human transcriptional coactivator hTIF1. *J. Biol. Chem.* **272,** 12062–12068
39. Tsai, W. W., Wang, Z., Yiu, T. T., Akdemir, K. C., Xia, W., Winter, S., Tsai, C. Y., Shi, X., Schwarzer, D., Plunkett, W., Aronow, B., Gozani, O., Fischle, W., Hung, M. C., Patel, D. J., and Barton, M. C. (2010) TRIM24 links a non-canonical histone signature to breast cancer. *Nature* **468,** 927–932
40. Klugbauer, S., and Rabes, H. M. (1999) The transcription coactivator HTIF1 and a related protein are fused to the RET receptor tyrosine kinase in childhood papillary thyroid carcinomas. *Oncogene* **18,** 4388–4393
41. Miao, Z. F., Wang, Z. N., Zhao, T. T., Xu, Y. Y., Wu, J. H., Liu, X. Y., Xu, H., You, Y., and Xu, H. M. (2015) TRIM24 is upregulated in human gastric cancer and promotes gastric cancer cell growth and chemoresistance. *Virchows Arch.* **466,** 525–532
42. Nihonmatsu-Kikuchi, N., Hashimoto, R., Hattori, S., Matsuzaki, S., Shinozaki, T., Miura, H., Ohota, S., Tohyama, M., Takeda, M., and Tatebayashi, Y. (2011) Reduced rate of neural differentiation in the dentate gyrus of adult dysbindin null (sandy) mouse. *PLoS One* **6,** e15886
43. Wang, H., Yuan, Y., Zhang, Z., Yan, H., Feng, Y., and Li, W. (2014) Dysbindin-1C is required for the survival of hilar mossy cells and the maturation of adult newborn neurons in dentate gyrus. *J. Biol. Chem.* **289,** 29060–29072
44. Elmore, S. (2007) Apoptosis: a review of programmed cell death. *Toxicol. Pathol.* **35,** 495–516
45. Hörnle, M., Peters, N., Thayaparasingham, B., Vörsmann, H., Kashkar, H., and Kulms, D. (2011) Caspase-3 cleaves XIAP in a positive feedback loop to sensitize melanoma cells to TRAIL-induced apoptosis. *Oncogene* **30,** 575–587
46. Hattangadi, D. K., DeMasters, G. A., Walker, T. D., Jones, K. R., Di, X., Newsham, I. F., and Gewirtz, D. A. (2004) Influence of p53 and caspase 3 activity on cell death and senescence in response to methotrexate in the breast tumor cell. *Biochem. Pharmacol.* **68,** 1699–1708
47. Ryu, Y. S., Lee, Y., Lee, K. W., Hwang, C. Y., Maeng, J. S., Kim, J. H., Seo, Y. S., You, K. H., Song, B., and Kwon, K. S. (2011) TRIM32 protein sensitizes cells to tumor necrosis factor (TNFα)-induced apoptosis via its RING domain-dependent E3 ligase activity against X-linked inhibitor of apoptosis (XIAP). *J. Biol. Chem.* **286,** 25729–25738
48. Liu, J., Zhang, C., Wang, X. L., Ly, P., Belyi, V., Xu-Monette, Z. Y., Young, K. H., Hu, W., and Feng, Z. (2014) E3 ubiquitin ligase TRIM32 negatively regulates tumor suppressor p53 to promote tumorigenesis. *Cell Death Differ.* **21,** 1792–1804
49. Jain, A. K., Allton, K., Duncan, A. D., and Barton, M. C. (2014) TRIM24 is a p53-induced E3-ubiquitin ligase that undergoes ATM-mediated phosphorylation and autodegradation during DNA damage. *Mol. Cell. Biol.* **34,** 2695–2709
50. Mullin, A. P., Gokhale, A., Larimore, J., and Faundez, V. (2011) Cell biology of the BLOC-1 complex subunit dysbindin, a schizophrenia susceptibility gene. *Mol. Neurobiol.* **44,** 53–64
51. Ghiani, C. A., and Dell'Angelica, E. C. (2011) dysbindin-containing complexes and their proposed functions in brain: from zero to (too) many in a decade. *ASN Neuro* **3,** e00058
52. Cohen, S., Zhai, B., Gygi, S. P., and Goldberg, A. L. (2012) Ubiquitylation by Trim32 causes coupled loss of desmin, Z-bands, and thin filaments in muscle atrophy. *J. Cell Biol.* **198,** 575–589
53. Kudryashova, E., Kudryashov, D., Kramerova, I., and Spencer, M. J. (2005) Trim32 is a ubiquitin ligase mutated in limb girdle muscular dystrophy type 2H that binds to skeletal muscle myosin and ubiquitinates actin. *J. Mol. Biol.* **354,** 413–424
54. Mokhonova, E. I., Avliyakulov, N. K., Kramerova, I., Kudryashova, E., Haykinson, M. J., and Spencer, M. J. (2015) The E3 ubiquitin ligase TRIM32 regulates myoblast proliferation by controlling turnover of NDRG2. *Hum. Mol. Genet.* **24,** 2873–2883

55. Kudryashova, E., Wu, J., Havton, L. A., and Spencer, M. J. (2009) Deficiency of the E3 ubiquitin ligase TRIM32 in mice leads to a myopathy with a neurogenic component. *Hum. Mol. Genet.* **18,** 1353–1367
56. Nicklas, S., Otto, A., Wu, X., Miller, P., Stelzer, S., Wen, Y., Kuang, S., Wrogemann, K., Patel, K., Ding, H., and Schwamborn, J. C. (2012) TRIM32 regulates skeletal muscle stem cell differentiation and is necessary for normal adult muscle regeneration. *PLoS ONE* **7,** e30445
57. Cohen, S., Lee, D., Zhai, B., Gygi, S. P., and Goldberg, A. L. (2014) Trim32 reduces PI3K-Akt-FoxO signaling in muscle atrophy by promoting plakoglobin-PI3K dissociation. *J. Cell Biol.* **204,** 747–758
58. Takahashi, R., Deveraux, Q., Tamm, I., Welsh, K., Assa-Munt, N., Salvesen, G. S., and Reed, J. C. (1998) A single BIR domain of XIAP sufficient for inhibiting caspases. *J. Biol. Chem.* **273,** 7787–7790
59. Scott, F. L., Denault, J. B., Riedl, S. J., Shin, H., Renatus, M., and Salvesen, G. S. (2005) XIAP inhibits caspase-3 and -7 using two binding sites: evolutionarily conserved mechanism of IAPs. *EMBO J.* **24,** 645–655
60. Hillje, A. L., Pavlou, M. A., Beckmann, E., Worlitzer, M. M., Bahnassawy, L., Lewejohann, L., Palm, T., and Schwamborn, J. C. (2013) TRIM32-dependent transcription in adult neural progenitor cells regulates neuronal differentiation. *Cell Death Dis.* **4,** e976
61. Le Douarin, B., Nielsen, A. L., Garnier, J. M., Ichinose, H., Jeanmougin, F., Losson, R., and Chambon, P. (1996) A possible involvement of TIF1α and TIF1β in the epigenetic control of transcription by nuclear receptors. *EMBO J.* **15,** 6701–6715
62. Costes, S. V., Daelemans, D., Cho, E. H., Dobbin, Z., Pavlakis, G., and Lockett, S. (2004) Automatic and quantitative measurement of protein-protein colocalization in live cells. *Biophys. J.* **86,** 3993–4003
63. Manders, E. M. M., Verbeek, F. J., and Aten, J. A. (1993) Measurement of colocalization of objects in dual-color confocal images. *J. Microsc.* **169,** 375–382
64. Dunn, K. W., Kamocka, M. M., and McDonald, J. H. (2011) A practical guide to evaluating colocalization in biological microscopy. *Am. J. Physiol. Cell Physiol.* **300,** C723–C742
65. Frank, D., Kuhn, C., Brors, B., Hanselmann, C., Lüdde, M., Katus, H. A., and Frey, N. (2008) Gene expression pattern in biomechanically stretched cardiomyocytes: evidence for a stretch-specific gene program. *Hypertension* **51,** 309–318